Component-based modelling of a novel ductile steel connection

Yu Liu[1*], Shan-Shan Huang[1] and Ian Burgess[1]

[1]*Department of Civil and Structural Engineering, University of Sheffield, Mappin Street, Sheffield S1 3JD, United Kingdom.*

*Corresponding Author: E-mail address: yliu230@sheffield.ac.uk (Yu Liu)

Abstract

To enhance the robustness of connections in fire, the improved design version of a novel ductile connection has been proposed. Performance of the improved design version of novel connection has been compared with that of the previous design version using a sub-frame model. The comparison results show that the improved version of novel connection further enhances its ductility. Five case studies have been carried out, in which the novel connections are applied to sub-frames with different beam spans. Results show that the axial forces generated in the beams with novel connections are significantly reduced compared with those of the beams with rigid connections. The analytical models for the web-cleat component of the novel connection and the WCSC component, which considers the semi-cylindrical section and the web-cleat as a whole to deform, have been developed based on simple plastic theory. Then two schemes of component-based model have been proposed for the novel ductile connection and loading and unloading behaviour have been incorporated into individual component. Result curves of the two schemes of component-based model have been compared and validated against Abaqus simulations and experiments. Finally, the proposed component-based model has been applied to two simple examples to illustrate how different spring rows work in the process of connection deformation.

Keywords: Ductility, steel connection, fire, component-based model

1. Introduction

Failure of connections in a fire accident may lead to the spread of fire to adjacent compartments, collapse of floors, buckling of columns, and even the progressive collapse of a whole steel-framed building. Traditional understanding of connection behaviour is limited to moment-rotation characteristics, which has been shown to be inadequate in fire conditions, due to the complex combinations of axial forces, shear forces and moments transferred between the connected structural members at elevated temperatures. It is difficult to reproduce such complex loading conditions in experiments, other than in full-scale tests. To investigate connection behaviour under the effects of degraded material properties, thermal expansion and combinations of forces, numerical modelling is a more feasible approach than simple member-by-member design. The finite element method is a reliable technique which enables prediction of the behaviour of connections in a very detailed manner under complex interactive conditions. It is also a much cheaper and easier way to conduct detailed investigations on a variety of connections of different sizes and types under different combinations of loads than experiments. Liu [1, 2] created models for extended flush endplates using shell elements for flanges and webs, and beam elements for bolts. Sarraj [3, 4] conducted a finite element parametric study, based on which he proposed equations to describe the bearing and shearing behaviour of fin-plate connections. Yu [5] used the explicit dynamic solver in Abaqus to analyse bolted steel connections of various types, and validated her simulation results against experiments previously done by AI-Jabri [6]. Dai [7] conducted a simulation study on restrained steel beam-column assemblies connected by five different joint types, including flexible endplate, flush endplate, web cleat, fin-plate and extended endplate connections. Garlock [8] evaluated the importance of slab in the response of single-plate shear connections and examined the effects of the rate of heating and cooling on the connections. However, due to the time-consuming nature of model building and computational runtimes, such detailed finite element approaches are not suitable to be used in practical fire engineering design of whole buildings, particularly where global frame analysis needs to be conducted. An alternative way of conducting large structural frame analyses in fire conditions involves the use of a component-based method to simulate connection behaviour, within a structural finite element program which is able to carry out non-linear analysis of structural behaviour under fire conditions.

The concept of the component-based method, which was initially used to describe the moment-rotation behaviour of steel-to-steel connections at ambient temperature, was first proposed in the 1980s [9] and

subsequently adopted in design guidance [10]. In the component-based method, the connection is considered as an assembly of basic components, each of which is represented by a non-linear spring. The force-deflection characteristics of components can include reduction of their material properties, as well as loading and unloading behaviour. Jaspart [11] summarized the three principal steps of representing a connection using the component-based method; identification of active components, evaluation of the analytical characteristics of each basic component and assembly of the active components. Leston-Jones [12] developed a high-temperature model for the rotational behaviour of flush endplate connection using components representing the column flange in bending, bolts in tension, endplate in bending and column web in compression. In this model the force-displacement curve of each component is tri-linear. The model was validated against high-temperature tests. Block [13] developed the high-temperature model for endplate connections, including components based on the analytical model of a T-stub developed by Spyrou [14] to represent the tension bolt rows and endplate of the connection. Block's model also included a simplified analytical model of the column web in compression to represent the compression zone of the connection. Continuing his work, Dong [15] developed a user-defined connection model, a flush endplate connection model and the reverse-channel connection model, all for elevated temperatures. In further developments at high temperatures Hu [16] developed the flexible endplate connection model, and Taib [17] developed the model for fin-plate connections based on the equations previously proposed by Sarraj[3, 4][3, 4][3, 4][3, 4][3, 4]. In general, the component-based method is a practical compromise between accuracy of results and computational cost compared with detailed FE modelling, and has therefore become more and more popular in recent years for ambient-temperature analytical design. In the case of structural frame, or sub-frame, analysis for fire conditions, it seems the only practically feasible way of taking account of connection behaviour within a 3-dimensional frame analysis.

Current connection types which are commonly used in steel-framed and composite buildings have insufficient ductility to accommodate the deformations generated by the connected beam, and to reduce forces such as the axial compression due to restrained thermal expansion during initial heating and the tension resulting from the catenary action of beams in the high-temperature phase of heating. A novel ductile connection was proposed by the author in a previous paper [18], which is intended to reduce connection forces and to prevent connection fracture in fire conditions. This paper presents an improved version of this connection and compare its performance with that of the previous version using a sub-frame model. Five

case studies are carried out, in which the novel connections are applied to sub-frames with different beam spans. The analytical model of the "web-cleat" component of the novel connection, and the web-cleat/semi-cylindrical component (WCSC) component, in which the semi-cylindrical component and the web-cleat component are considered to deform as a whole, based on simple plastic theory are developed. Based on these, two component-based models for the novel connection have been proposed. The loading and unloading behaviour have been incorporated into individual component behaviour, and the results of the two component-based models are compared and validated against both Abaqus simulations and experiments. Finally, the proposed component-based model is applied to two simple examples, to illustrate how different spring rows contribute to the process of connection deformation.

2. Design and application of the novel connection

2.1 Optimized design of the novel connection

The ductility of connections is vital for a structure to retain its integrity and stability under exposure to fire. A novel ductile connection has been proposed in the previous paper [18] to meet the ductility demands induced by the large deformation of long-span steel beams in fire conditions. The connection proposed consists of two identical parts, each of which takes the form of a fin-plate which is bolted to the beam web, an end-plate which is bolted to either the column web or flange, with a semi-cylindrical section between the fin-plate and end-plate. The semi-cylindrical section is the key part in providing the required axial ductility by allowing the fin-plate to move towards and away from the end-plate.

The basic element of this connection can be manufactured simply by bending a steel plate. In order to facilitate this cold formation, the design proposed in the previous paper has been modified as shown in Figure 1. The sharp intersection between the semi-cylindrical part and end-plate has been replaced by a curve of higher radius in order to reduce the plastic residual strains induced by bending.

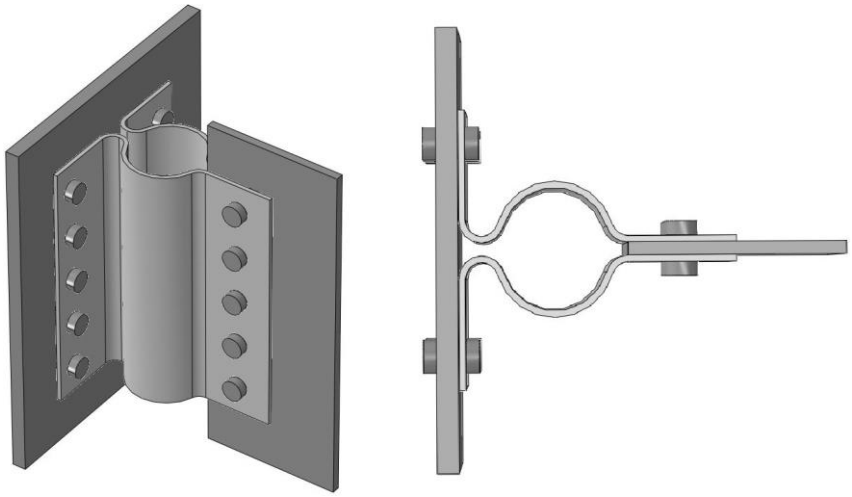

Figure 1. Design of the novel ductile connection.

To check whether this change of specification causes unforeseen changes in behaviour, a simple two-storey three-bay plane steel frame, shown in Figure 2, has been modelled using Abaqus. The dimensions of the original and modified connections are shown in Figure 3. Fire is assumed to occur only in the ground floor of the central bay. The two adjacent cold bays on both sides can, therefore, be simplified as elastic horizontal springs with known axial stiffness, which can be calculated using Equation (1). Only half of the central bay is created in the Abaqus model to save computational cost. A uniform line transverse load is applied to the beam's top flange, generating a load ratio of 0.5, which is slightly larger than typical values for the Fire Limit State, with respect to simply supported beams.

$$K = \frac{1}{2 / K_{connection} + 1 / K_{column}} \tag{1}$$

in which K_{column} and $K_{connection}$ respectively represent the lateral sway stiffness of a perimeter column and the axial push-pull stiffness of the connections in the outer bays.

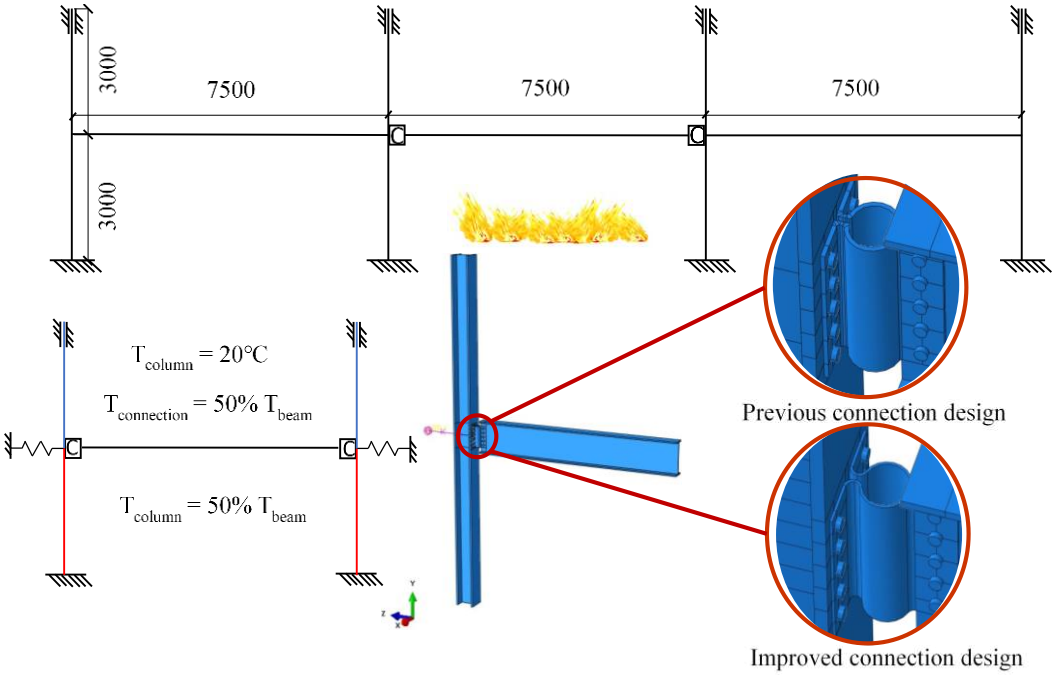

Figure 2. Sub-frame model (all dimensions in mm).

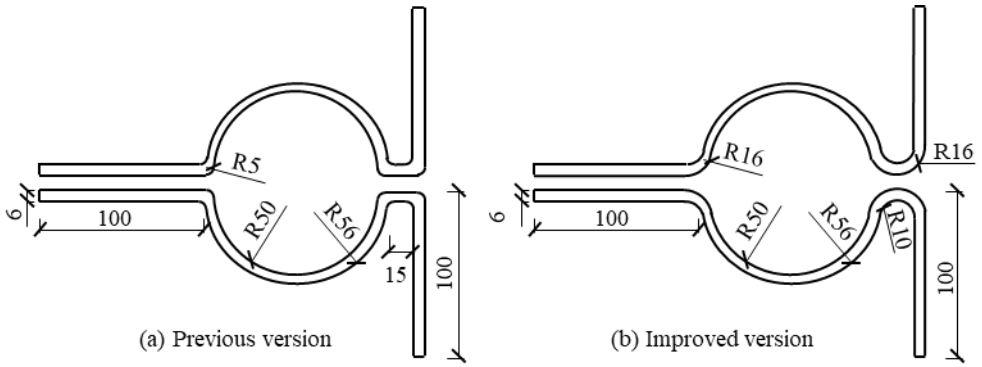

Figure 3. Dimensions of the two versions of connection (all dimensions in mm).

Comparing results from the frame with the previous connection design and the same frame with the improved connection design are shown in Figure 4 and Figure 5. It can be seen from Figure 4 that the solid curve representing the mid-span deflection of the beam with the improved design of connections is very close to that of the beam with previous version of connections, represented by the dashed line. The comparison of axial forces (shown in Figure 5) shows that the axial force generated in the beam with the improved version of connections is much smaller than that of the beam with the old version of connections. This indicates the significantly enhanced deformability and ductility of the new design, as expected during the redesigning of the connection.

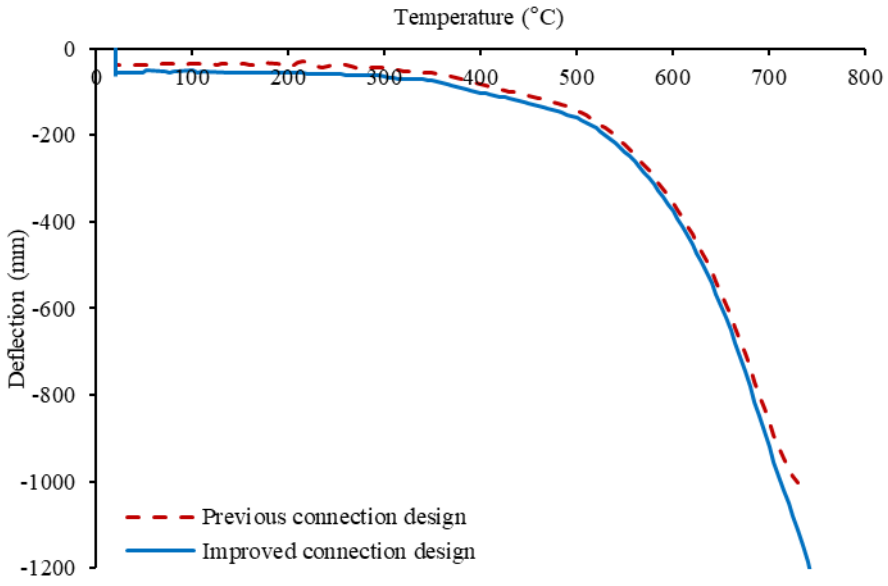

Figure 4. Deflection at beam mid-span.

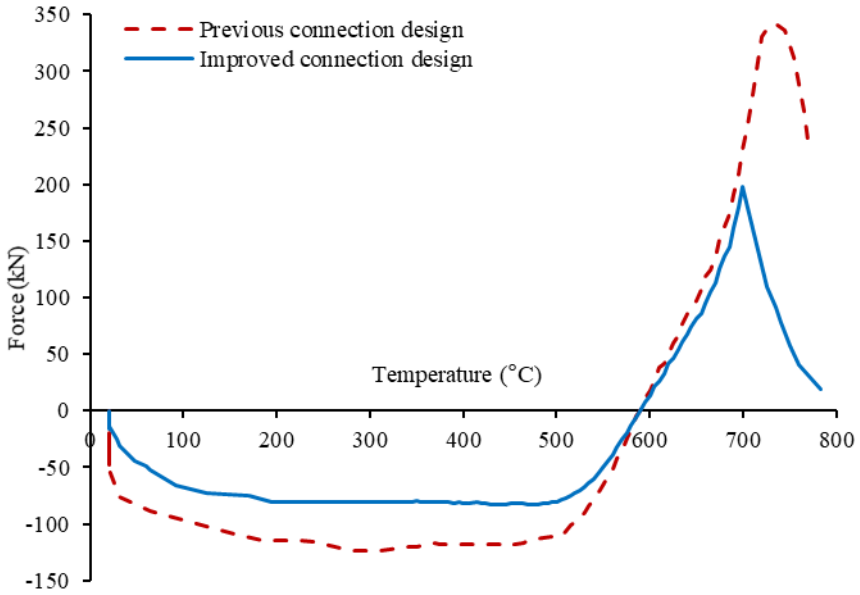

Figure 5. Axial force of beam.

2.2 Application of the novel connection

In this section, the sub-frame shown in Figure 2 is used to conduct case studies, as a preliminary demonstration of the novel connection in building frames. Various beam spans (from 6m to 12m) are considered. A uniformly distributed line load of 42.64 kN/m is applied on the beam and the load ratio of 0.4 is adopted in all cases. The selected beam sizes based on span and load ratio are shown in Table 1. A UKC 305 ×305×198 is selected for the columns for all cases.

As mentioned previously, the semi-cylindrical section of the connection is critical in providing the required ductility. The radius of this section should not be too small, otherwise, the ductility will be reduced and the axial force generated in the adjacent structural members will be increased. Therefore, the radius of the semi-cylindrical section should be determined according to the ductility demand of the connected beam during a fire event (as shown in Figure 6), which can be calculated using Equations (2) – (4), which were proposed in the previous paper [18]. The diameter of semi-cylindrical section should be larger than the maximum value of $\Delta_{low-temp}$, $\Delta_{high-temp}$ and $\Delta_{high-temp,\max}$. The fin-plate and the end-plate of the novel connection can be designed based on Eurocode [10]. The dimensions of the novel connections for all cases are shown in Table 2. The connections must be adequate for ambient-temperature Ultimate Limit State conditions. Therefore, the capacities of the connections have all been checked according to the Eurocode [10], which include shear capacity of the semi-cylindrical section, bolt shear capacity, bolt bearing capacity, shear and bearing capacity of the fin-plate, shear and bearing capacity of the bolt group and shear capacity of the end-plate.

$$\Delta_{low-temp} = \frac{1}{2}(\alpha l T + h\theta) - \frac{4}{3}\delta^2 / l \tag{2}$$

$$\Delta_{high-temp} = \frac{4}{3}\delta_{\max}{}^2 / l - \frac{1}{2}(\alpha l T + h\theta) \tag{3}$$

$$\Delta_{high-temp,\max} = \frac{4}{3}\delta_{\max}{}^2 / l - \frac{1}{2}(\alpha l T - h\theta) \tag{4}$$

in which α is the thermal expansion coefficient of steel, T is the beam temperature, l is the length of the beam, h is the height of the beam section and δ is the mid-span deflection of the beam.

Table 1. Beam sizes and ductility demands

Span (mm)	Beam section	Load ratio	$\Delta_{low-temp}$ (mm)	$\Delta_{high-temp}$ (mm)	$\Delta_{high-temp,\max}$ (mm)
6000	UKB 457×152×82	0.40	23.74	7.85	72.90
7500	UKB 533×210×109	0.40	29.61	11.86	76.54
9000	UKB 533×312×151	0.39	35.28	20.00	57.39
10500	UKB 610×305×179	0.40	41.22	24.17	62.78
12000	UKB 610×305×238	0.39	46.88	37.08	39.70

Table 2. Connection sizes

Span (mm)	Inner radius of semi-cylindrical section (mm)	Plate thickness (mm)	Fin-plate width (mm)×depth (mm)	End-plate width (mm)×depth (mm)	Number of bolt rows
6000	50	6	100×360	100×360	5
7500	50	6	100×360	100×360	5
9000	50	6	100×360	100×360	5

10500	50	6	120×430	100×430	6
12000	50	6	120×430	100×430	6

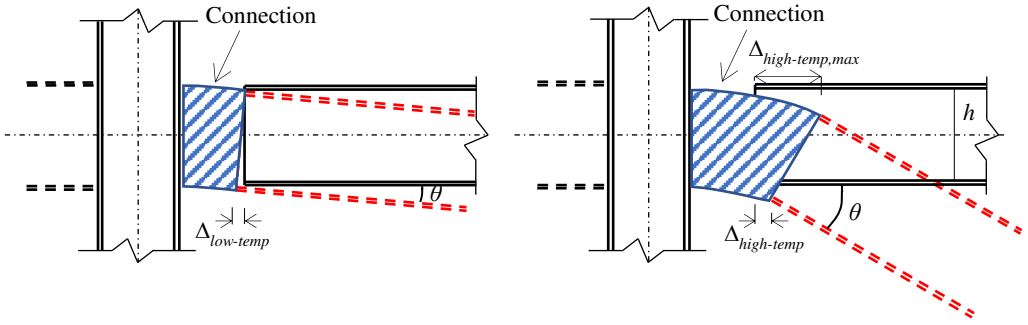

Figure 6. Ductility demand of a beam during a fire event[18]

Mid-span deflections and the axial forces of the beams are shown in Figure 7 (a) and (b). In order to compare the performance of the novel connections with that of the commonly-used end-plate connections, the five sub-frames, whose novel connections are replaced by end-plate connections, are also simulated using Abaqus. In extreme cases, if the beam is fully restraint in axial direction without buckling, then the axial forces generated in the beams during the initial stage of heating can be simply calculated by the Hooke's law (Equation (5)). The comparison results of the axial forces generated in the beams under different axial restraint conditions, the novel connection, the end-plate connection and the axial fully restraint without buckling, at the temperature of 400℃ are shown in Table 3. It is obvious that the axial compressive forces generated in the beams are significantly reduced by adopting the novel connections. The horizontal displacements of the node on the top flange and the node on the bottom flange at the beam end are shown in Figure 7 (c) and (d). These two figures clearly show the deformation capacity of the novel connection, which can allow the connected beam to fully develop its catenary action at high temperatures. As can be seen from the case studies presented in this section, the novel connections are quite suitable for bare-steel frames with different beam spans. It should be noted that the radius of the semi-cylindrical section of the novel connection is the most important parameter, being based on the demand for push-pull ductility. This should be determined according to the span of beam, its size, applied load and required fire resistance temperature, using Equations (2) – (4). The novel connection should also be applicable to composite structures, but the behaviour of connections within a composite floor is quite different from that in a non-composite steel frame, due to the influence of the concrete slab in resisting thermal expansion of the beam. Performance of the novel connections within composite structures will be studied in the future.

$$F_N = E \cdot A \cdot \alpha \cdot T \tag{5}$$

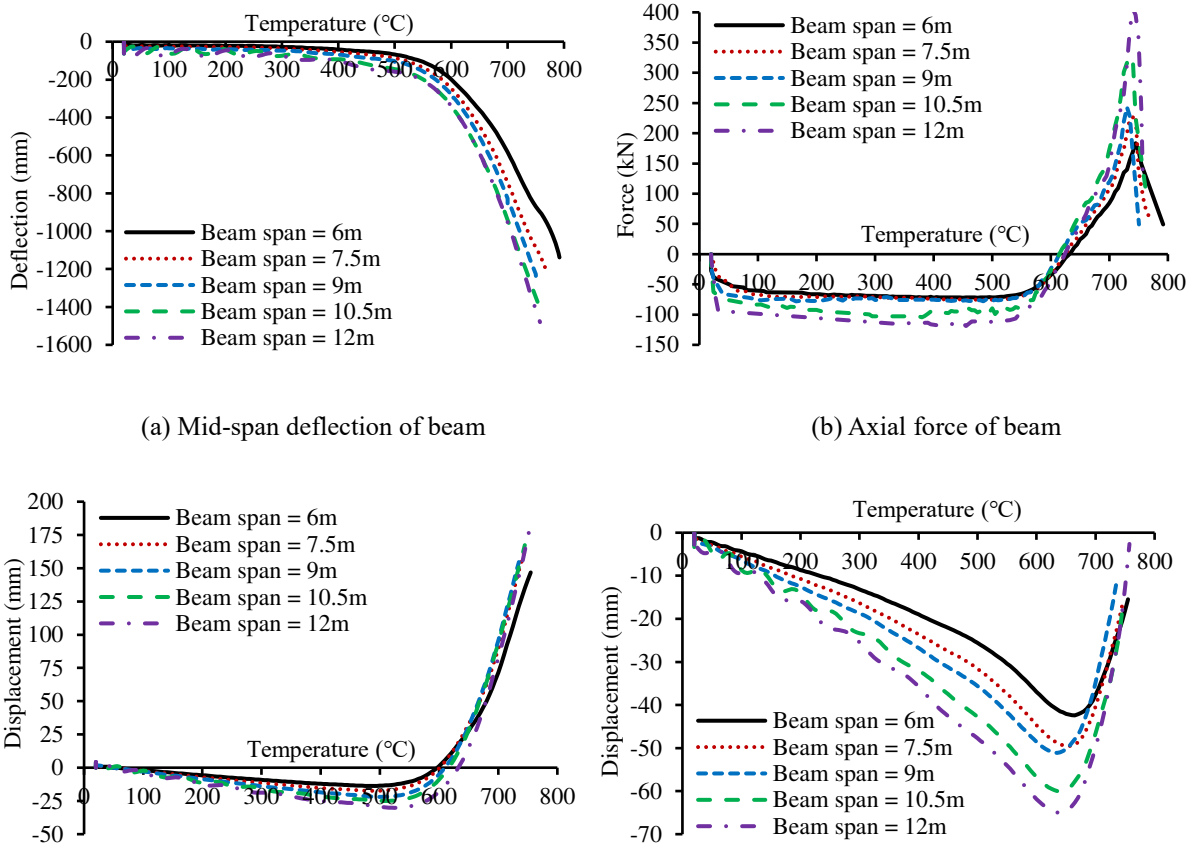

(a) Mid-span deflection of beam

(b) Axial force of beam

(a) Horizontal displacement of top flange at beam end

(b) Horizontal displacement of bottom flange at beam end

Figure 7. Results of case studies

Table 3. Comparison of the compressive axial forces of the beams at 400°C

Beam span (m)	Axial force (novel connections)	Axial force (end-plate connections)	Axial force (axial fully restraint)
6	-71.41 kN	-824.42 kN	-3285.01 kN
7.5	-75.52 kN	-985.28 kN	-4348.72 kN
9	-77.18 kN	-1139.47 kN	-6006.87 kN
10.5	-89.52 kN	-1152.98 kN	-7133.16 kN
12	-112.24 kN	-1328.10 kN	-9479.59 kN

3. Initial component-based model

The new connection design consists of a fin-plate, a semi-cylindrical section and a web-cleat. The active components of the component-based connection model are shown in Figure 8. Each spring row of the component-based model consists of five components working in series. Among them, the fin-plate in bearing, beam-web in bearing and bolt in shear constitute the Fin-plate component; characterisation of these components has been done previously [4]. The gap between the compression spring row and the rigid bar is

designed to represent the maximum compressive displacement before contact occurs. The two end nodes of the connection element are located at the intersection point between the reference axes of the beam and column. The vertical shear behaviour, representing the slip between the beam end and the column flange, has not been taken into consideration, although this will be an issue to be investigated since it is relevant to ambient-temperature design. Therefore, the component-based model is assumed to be rigid in the vertical direction.

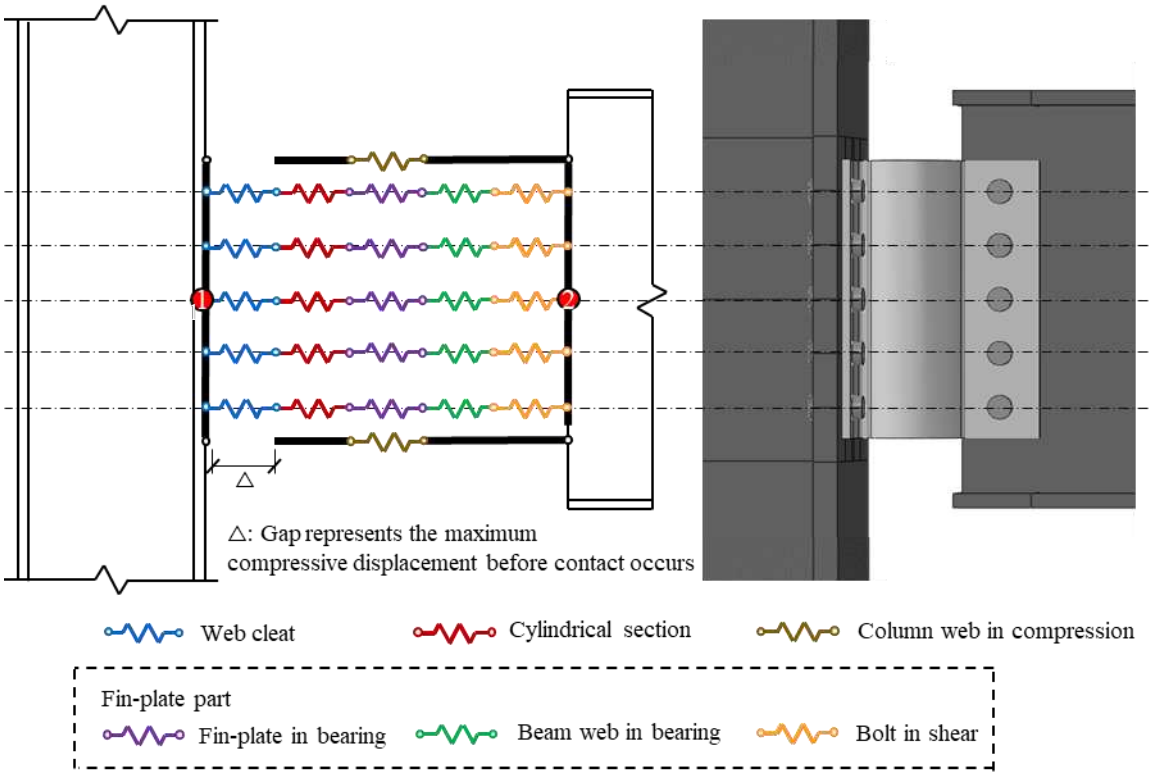

Figure 8. First scheme of the component-based model.

3.1 Analytical model of the semi-cylindrical component

An analytical model of the semi-cylindrical component was developed in the previous paper [18] and Equations (6)-(9) are directly used here to generate the force-displacement curve of this component. A bi-linear stress-strain relationship is assumed at ambient temperature, changing to a tri-linear constitutive law for elevated temperatures. Two key points, (ε_y , f_y) and (ε_u , f_u) are used to define the tri-linear stress-strain relationship, where ε_y , f_y , ε_u and f_u represent the yield strain, yield stress, ultimate strain and ultimate stress, respectively. When the stress reaches its ultimate value f_u , the stress no longer increases with increase of strain. Full details of these two stress-strain relationships are documented in Reference [18]. It can be seen

from these equations that the pulling/pushing force increases with the increase of plate thickness. This means that the ductility of the connection decreases with the increase of plate thickness. However, due to the shear capacity requirements of the novel connection, the plate thickness should not be too small.

For the bi-linear stress-strain relationship at ambient temperature:

When $\varepsilon_m \le \varepsilon_y$ $F = \dfrac{Eht^2\theta}{6r\left[\cos(\theta/n) - \sin(\theta+\alpha)\right]}$ (for pulling)

$$F = \frac{Eht^2\theta}{6r\left[\sin(\theta-\alpha) + \cos\theta\right]} \text{ (for pushing)} \tag{6}$$

When $\varepsilon_m > \varepsilon_y$ $F = \dfrac{ht^2\left[3\theta^2 f_y - \left(12 f_y \varepsilon_y^2 - 8E\varepsilon_y^3\right)\right]}{6\theta^2 r\left[\cos(\theta/n) - \sin(\theta+a)\right]}$ (for pulling)

$$F = \frac{ht^2\left[3\theta^2 f_y - \left(12 f_y \varepsilon_y^2 - 8E\varepsilon_y^3\right)\right]}{6\theta^2 r\left[\sin(\theta-\alpha) + \cos\theta\right]} \text{ (for pushing)} \tag{7}$$

For the tri-linear stress-strain relationship at elevated temperatures:

When $\varepsilon_m \le \varepsilon_y$, the equation is the same as that for the bi-linear material.

When $\varepsilon_y < \varepsilon_m \le \varepsilon_u$ $F = \dfrac{ht^2\left[E_t\theta^3 + (E-E_t)(3\theta^2\varepsilon_y - 4\varepsilon_y^3)\right]}{6\theta^2 r\left[\cos(\theta/n) - \sin(\theta+\alpha)\right]}$ (for pulling)

$$F = \frac{ht^2\left[E_t\theta^3 + (E-E_t)(3\theta^2\varepsilon_y - 4\varepsilon_y^3)\right]}{6\theta^2 r\left[\sin(\theta-\alpha) + \cos\theta\right]} \text{ (for pushing)} \tag{8}$$

When $\varepsilon_m > \varepsilon_u$ $F = \dfrac{ht^2\left[3\theta^2 f_u + (E-E_t)(3\varepsilon_y\varepsilon_u^2 - \varepsilon_y^3) + 2E_t\varepsilon_u^3 - 3f_u\varepsilon_u^2\right]}{6\theta^2 r\left[\cos(\theta/n) - \sin(\theta+\alpha)\right]}$ (for pulling)

$$F = \frac{ht^2\left[3\theta^2 f_u + (E-E_t)(3\varepsilon_y\varepsilon_u^2 - \varepsilon_y^3) + 2E_t\varepsilon_u^3 - 3f_u\varepsilon_u^2\right]}{6\theta^2 r\left[\sin(\theta-\alpha) + \cos\theta\right]} \text{ (for pushing)} \tag{9}$$

3.2 Analytical model of the web-cleat component

Simple plastic theory is adopted here to model the plastic behaviour of the web-cleat component, considering both material and geometric nonlinearities. The relationship between the applied force and displacement of the web-cleat component is obtained based on the virtual work principle. The calculation of

the strain energy of plastic hinges is documented in the previous paper, and so it is not described here.

The geometric relationship illustrated in Figure 9 between the displacements and the rotation angles of the plastic hinges is the key to solving the virtual work equation. It is assumed that the bolt connected to the column flange provides full fixity, and therefore the fixed-point A is located at the edge of the bolt head. The deformation of the web-cleat can be divided of two steps. The leg of web-cleat, represented by AB in Figure 9, first rotates by the angle θ. The arc section CE then deforms to a straight horizontal section in the second step. This can be achieved by rotating angles $\theta/4$ and $\theta/2$ at the hinge C and hinge D respectively, if the arc section CE is divided into 2 segments (N=2). For the more general case, if the arc section CE is divided into N segments, the first hinge rotate $\theta/2N$ and the other hinges rotate 2*($\theta/2N$) at the second step. The total horizontal displacement can then be calculated as:

$$\Delta = \Delta_1 + \Delta_2 + \Delta_3 = \left(L\sin\theta - r\right) + r\cos\theta + 2Nr\sin\left(\frac{\theta}{2N}\right) \tag{10}$$

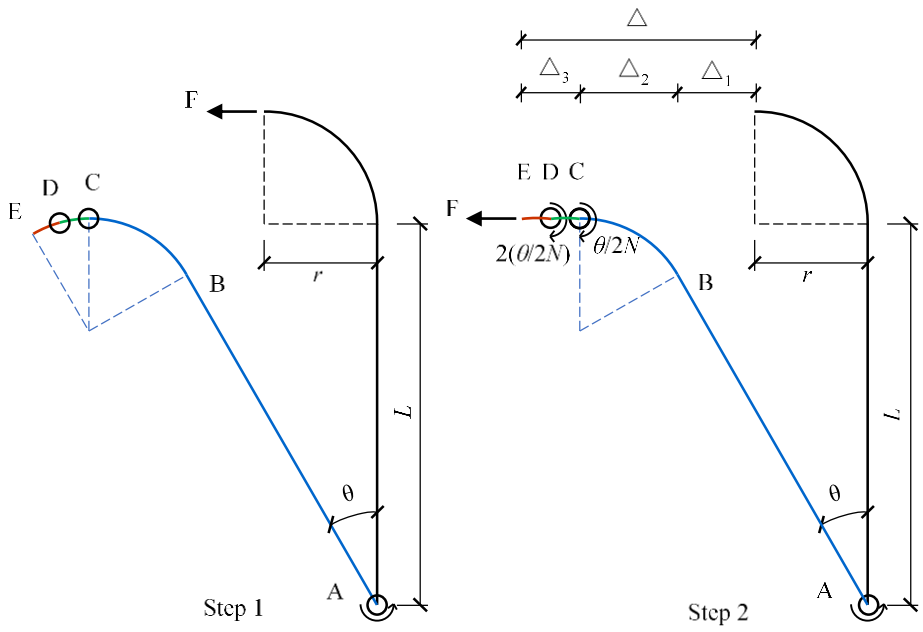

Figure 9. Geometric relationships.

Then the relationship between the horizontal force and displacement can be obtained by solving the virtual work equation. For bi-linear material at ambient temperature:

When $\varepsilon_m \le \varepsilon_y$: $$F = \frac{Eht^2\theta}{12\left[L\cos\theta - r\sin\theta + r\cos\left(\frac{\theta}{2N}\right)\right]} \cdot \frac{4N-1}{2N} \tag{11}$$

When $\varepsilon_m > \varepsilon_y$: $$F = \frac{ht^2\left[3\theta^2 f_y - \left(12 f_y \varepsilon_y^2 - 8E\varepsilon_y^3\right)\right]}{12\theta^2\left[L\cos\theta - r\sin\theta + r\cos\left(\frac{\theta}{2N}\right)\right]} \cdot \frac{4N-1}{2N} \tag{12}$$

where h is the width of web-cleat, E is Young's modulus, ε_m is the maximum strain of plastic hinge, ε_y and f_y are yield strain and stress, respectively.

For tri-linear material at elevated temperatures:

When $\varepsilon_m \le \varepsilon_y$, equation is the same as that in the case of bi-linear material.

When $\varepsilon_y < \varepsilon_m \le \varepsilon_u$: $$F = \frac{ht^2\left[E_t\theta^3 + (E - E_t)(3\theta^2\varepsilon_y - 4\varepsilon_y^3)\right]}{6\theta^2\left[L\cos\theta - r\sin\theta + r\cos\left(\frac{\theta}{2N}\right)\right]} \frac{4N-1}{2N} \tag{13}$$

When $\varepsilon_m > \varepsilon_u$: $$F = \frac{ht^2\left[3\theta^2 f_u + (E - E_t)(3\varepsilon_y\varepsilon_u^2 - \varepsilon_y^3) + 2E_t\varepsilon_u^3 - 3f_u\varepsilon_u^2\right]}{12\theta^2\left[L\cos\theta - r\sin\theta + r\cos\left(\frac{\theta}{2N}\right)\right]} \frac{4N-1}{2N} \tag{14}$$

where E_t is tangent stiffness, ε_u and f_u are ultimate strain and stress, respectively.

A sensitivity analysis on the value of N has been carried out at ambient temperature, and the results are shown in Figure 10. As shown in this figure, adequate convergence is achieved when N is larger than 10, and this value is, therefore, used in subsequent calculations.

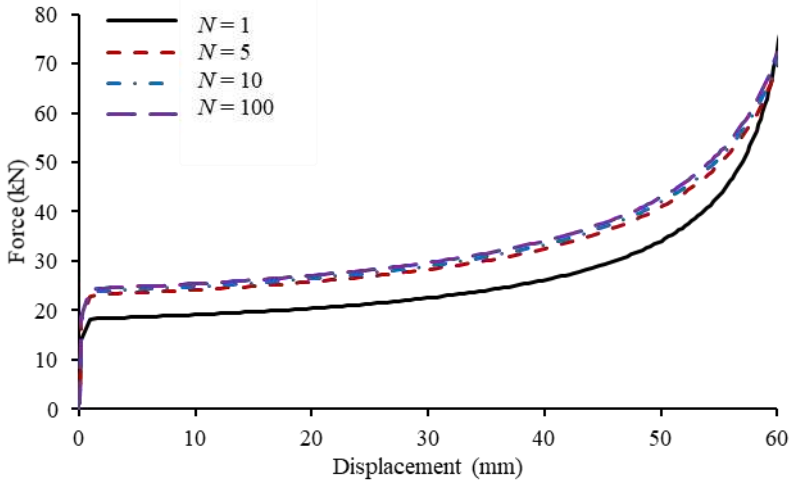

Figure 10. Influence of N value on analytical model.

3.3 Fin-plate component and column web in compression

The fin-plate component of the connection consists of three components, including fin-plate in bearing, beam web in bearing and bolt in shear. Sarraj [4] carried out a finite element parametric study, based on which, he proposed Equation (15) to describe the normalised force-displacement curves of the bearing components using different curve-fit values Ψ and Φ.

$$\frac{F}{F_{b,rd}} = \frac{\Psi\bar{\Delta}}{(1+\bar{\Delta}^{0.5})^2} - \Phi\bar{\Delta} \tag{15}$$

where $F_{b,rd}$ is the nominal plate strength and $\bar{\Delta}$ is the normalised bolt hole bearing deformation. Sarraj [4] also developed a modified Ramberg-Osgood expression, Equation (16), to represent the relationship between force and bolt shear deformation. Equations (15) and (16) are adopted in this work to generate the force-displacement curves of fin-plate in bearing, beam web in bearing and bolt in shear.

$$\frac{F}{K_{v,b}} + \Omega\left(\frac{F}{F_{v,rd}}\right)^m = \Delta \tag{16}$$

Where $K_{v,b}$ is the shear stiffness of a bolt, and $F_{v,Rd}$ is its shear strength. The index *m* controls the curvature of the response curve. As for the column web in compression, the force-displacement curve proposed by Block [13] is adopted in this component-based model. This compression curve is divided into elastic and plastic parts, represented by Equations (17) and (18), respectively.

When $\delta \le \delta_{el}$: $F = \delta k_T$ (17)

When $\delta_{el} < \delta \le \delta_u$: $F = F_{el} - c + \frac{b}{a}\sqrt{a^2 - (\delta_u - \delta)^2}$ (18)

where k_T is the tangent stiffness of elastic part and is calculated using the parameters *a, b* and *c*. The detailed calculations of k_T , *a, b* and *c* can be found in Reference [13].

3.4 Loading and unloading process of spring row

When the connection deforms, the forces in each component of a spring row are identical, and the deformation of the whole spring row is the sum of deformations of all components. The resistance of each spring row is governed by the weakest component in this series.

3.4.1 Unloading at constant and changing temperatures

Irreversible deformation occurs when the deformation of a component enters the plastic range. Block [13] and Dong [15] employed the classic Masing rule [19], based on which the unloading curve is obtained by doubling the loading curve in scale and rotating by 180°, to represent this 'memory effect'. However, since the tension and compressive curves of the semi-cylindrical component are not identical in shape [18], the Masing rule is not suitable for this connection. The unloading path of the proposed connection is simplified to be linear, with slope equal to that of the initial linear-elastic part of the loading curve, as shown in Figure 11.

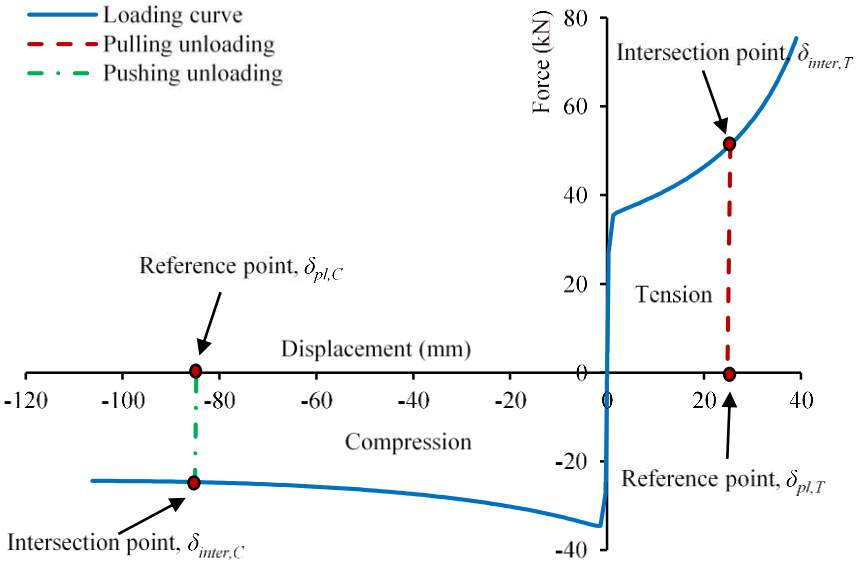

Figure 11. Unloading at constant temperature.

The intersection between the unloading path and the horizontal-axis is defined as the Reference Point, representing the permanent deformation caused at zero force. The intersection of the unloading path and the loading curve is defined as the Intersection Point. Displacement control is adopted to calculate the force-displacement response of the component-based model. During the calculation process, the displacement of the intersection point δ_{inter} and that of the reference point δ_{pl} at the end of each displacement step is stored. If the applied displacement at an arbitrary step δ is larger than δ_{inter}, the loading path will be followed and the permanent deformation will be updated accordingly. Therefore, both the intersection point and reference point are updated at the end of this step. If δ is less than δ_{inter} but larger than the δ_{pl}, the unloading path will be followed and the permanent deformation will not change. If δ is less than δ_{pl}, the push-back curve for tension or the pull-back curve for compression will be followed (see details in Section 3.4.2).

When the connection is exposed to fire, its temperature changes continuously, and the force-displacement relationships of the components are temperature-dependent. The 'Reference Point' concept is introduced to generate the unloading curve of each component at changing temperatures. This concept, assuming that plastic strain is not affected by the change of temperature, was initially used by Franssen [20] to describe the unloading behaviour of composite beams and columns, and by El-Rimawi [21] to describe the cooling behaviour of steel beams and columns. Bailey [22] used the concept to incorporate unloading into the simple moment-rotation connection spring element in the early version of Vulcan. Continuing his work, Block [13] and Dong [15] also adopted the concept in the development of the endplate and reverse-channel connection elements. When using this concept to describe the unloading behaviour of a component at changing temperatures, all force-displacement curves at different temperatures unload to the same Reference Point, as shown in Figure 12. At 20℃, the semi-cylindrical component is loaded to a displacement δ_1, generating a permanent deformation δ_{pl}. In the next step, it is assumed that the temperature of connection changes to 600℃, and the applied displacement at this step is δ_2. The corresponding force F_2 needs to be calculated in three steps. The first step is to generate the force-displacement curve at 600℃. The second is to calculate the intersection point (δ_{inter}, F_{inter}) using the displacement at the reference point δ_{pl} of the previous step at 20℃ and the slope of the linear-elastic part of the loading curve at 600℃. The final step is to determine which force-displacement relationship (loading, unloading, push-back or pull-back) should be used for the calculation of force F_2, on the basis of the relationship between δ_2, δ_{inter} and δ_{pl}.

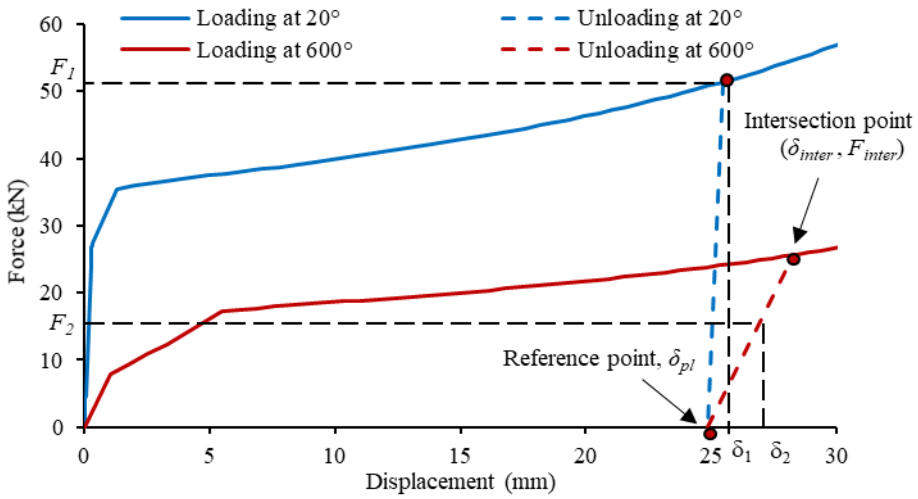

Figure 12. Unloading with changing temperatures.

3.4.2 Combined loading and unloading curve of each spring row

Figure 13 shows the calculation procedure for each spring row. The force-displacement curves of all five components (springs) in each spring row are combined into one force-displacement relationship based on the fact that these springs work in series. At an arbitrary force level, the displacement of the combined force-displacement curve is the sum of the displacements of all components under this force. The loading and unloading process has been described in detail in Section 3.4.1. The maximum deformation limit of a spring row during pulling is reached when any component in a row reaches its failure force. In the loading stage, this deformation limit is checked, as shown in the flowchart of Figure 13. If the deformation limit is not reached, the force and displacement of this spring row will be output and the corresponding displacement of the Reference Point of each component will be updated. Otherwise, this spring row is considered as having failed and is deactivated. A spring row is pushed back from tension, or pulled back from compression, when the applied displacement in a new displacement step is less than the displacement of the reference point δ_{pl} of the previous step. The combined push-back or pull-back curve needs to be determined. The push-back and pull-back curves of the semi-cylindrical component can be obtained using the compression and tension analytical models developed in previous paper [18], together with the existing deformation of the connection. The push-back curve of the web-cleat can be obtained using the same method described in Section 3.1, except that the deformation of the already deformed connection should be considered. Following this procedure, the complete force-displacement relationship under cyclic load of an example connection of the size shown in Figure 3 (b), fabricated in steel of grade S275, is established, as shown in Figure 14. The blue loop starts in pulling, and then the connection is unloaded and pushed-back to its original state. As shown in Figure 14, during push-back, the force increases sharply when the displacement is around 10mm. This is because the maximum force of the push-back curve of the web-cleat component is smaller than that of the push-back curve of the semi-cylindrical component, and so the web-cleat component will be pushed back to its original position first. The push-back of the semi-cylindrical component then causes the sudden increase in force. The red loop starts in pushing. The connection is then unloaded and pulled back to its original shape.

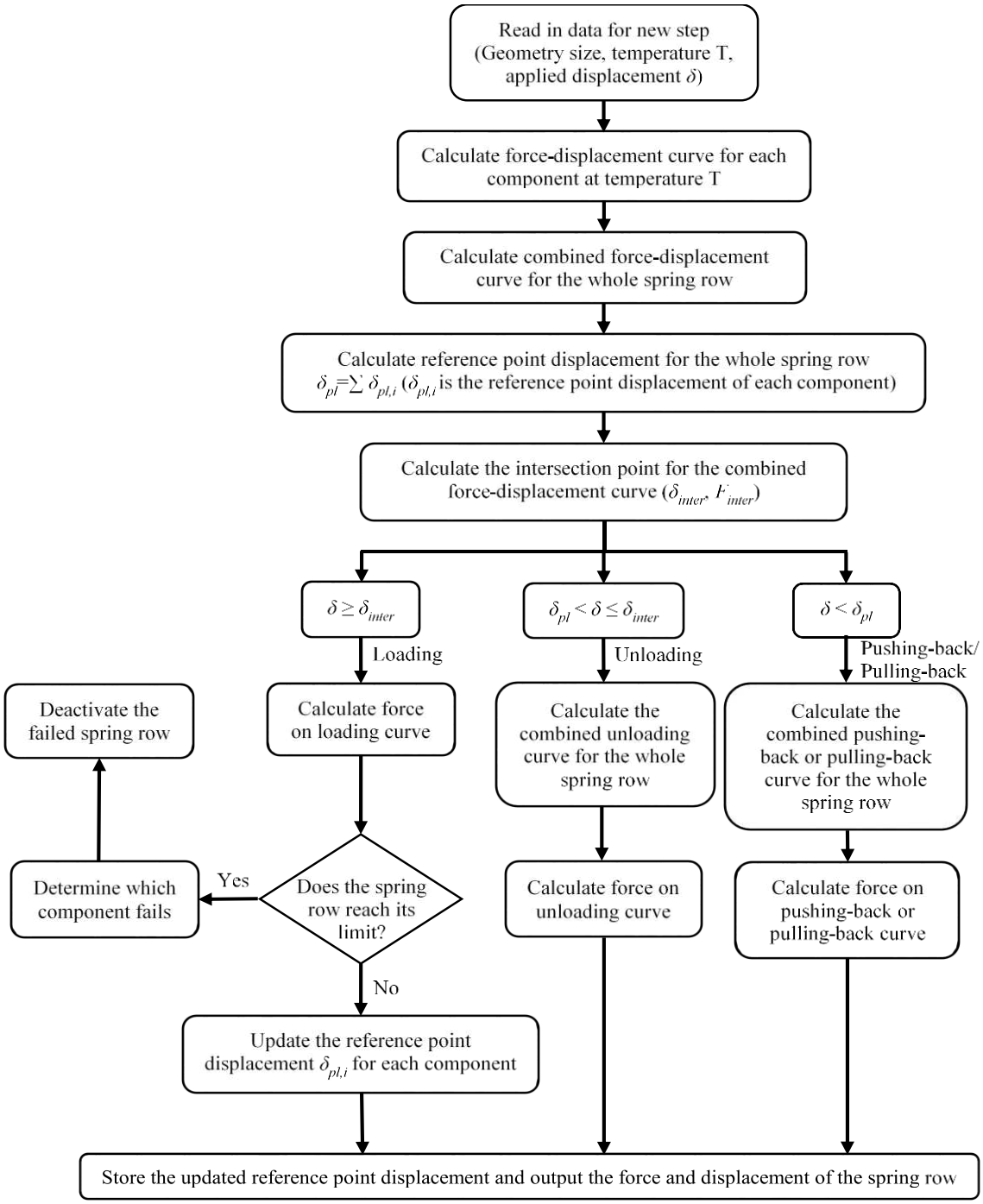

Figure 13. Calculation procedure for each spring row.

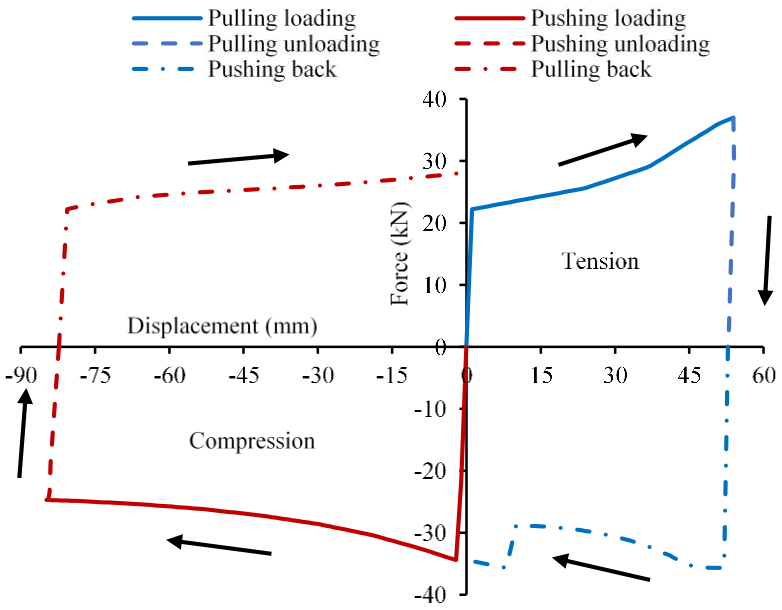

Figure 14. Loading and unloading process for a spring row.

4. Alternative component-based model

In the scheme given in Section 3 for the component-based model, the semi-cylindrical section and the web-cleat are treated as two separate components, working in series. However, in the actual deformation process, these two parts of the connection interact with each other directly. Therefore, a web-cleat/semi-cylindrical (WCSC) component is adopted as an improved scheme for the component-based model. This considers the semi-cylindrical section and the web-cleat as a single component, as shown in Figure 15. Two deformation cases generally need to be considered when developing the WCSC component, according to the position of the web-cleat bolts; these are described below.

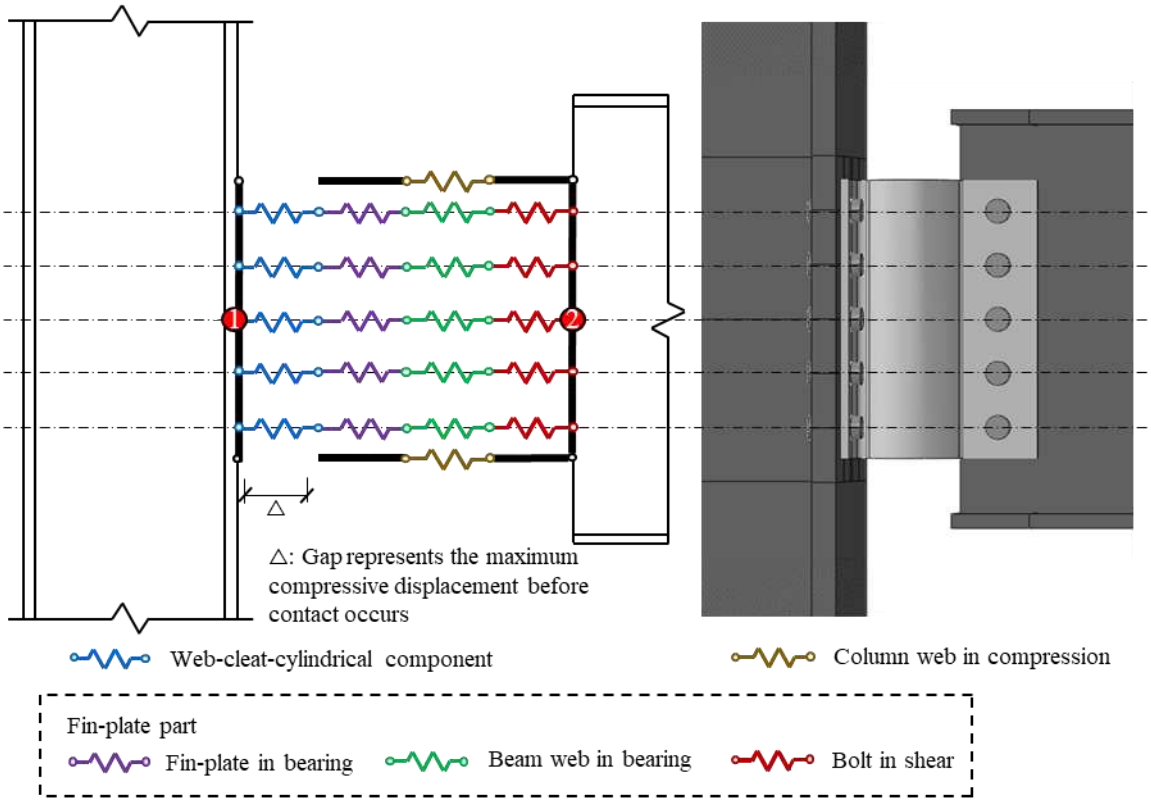

Figure 15. Second scheme of the component-based model.

4.1 Case 1 of the WCSC component

In Case 1, the length of the web-cleat leg from the edge of the bolt head to the initial plate bend is larger than the radius of the semi-cylindrical section. It is assumed that five plastic hinges can be formed during the deformation of the component, which are located at the two ends and outer edge (considered as two adjacent hinges) of the semi-cylindrical section, and the edge of bolt head, as shown in Figure 16. The position of the bolt is indicated by L_2; this is 99.6 mm for the example component. The dimensions of the example WCSC component analysed here are shown in Figure 3 (b).

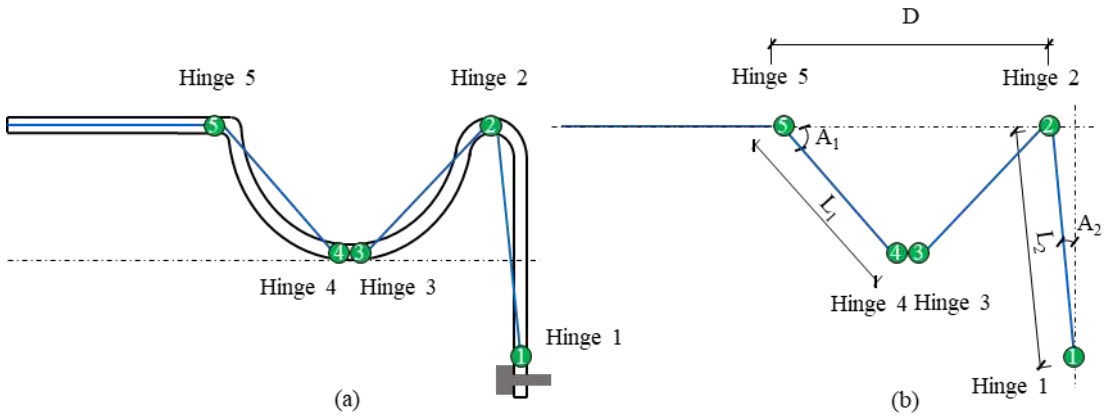

Figure 16. Schematic diagram of Case 1.

4.1.1 Pulling

The pulling of the WCSC component can be divided into two stages. In the first stage, only Hinges 1, 2 and 5 rotate; in the second stage, all the plastic hinges rotate, as shown in Figure 17. In both stages, the rotation of one (the "control" hinge) of the five hinges is firstly assumed; the rotations of the other hinges are then calculated. Assuming that the rotation of the control hinge is θ, the sum of the rotation angles of all plastic hinges and the total horizontal displacement are functions of θ. According to the virtual work principle:

$$F \cdot d\Delta(\theta) \cdot d\theta = M_P\left[A(\theta)\right] \cdot dA(\theta) \cdot d\theta \tag{19}$$

where $\Delta(\theta)$ is the total horizontal displacement, $M_P\left[A(\theta)\right]$ is the plastic moment, and $A(\theta)$ is the sum of the rotations of all plastic hinges. The calculation of plastic hinge moment has been documented in the previous paper [18]. The relationship between force and displacement is obtained from:

$$F = \frac{M_P\left[A(\theta)\right] \cdot dA(\theta)}{d\Delta(\theta)} \tag{20}$$

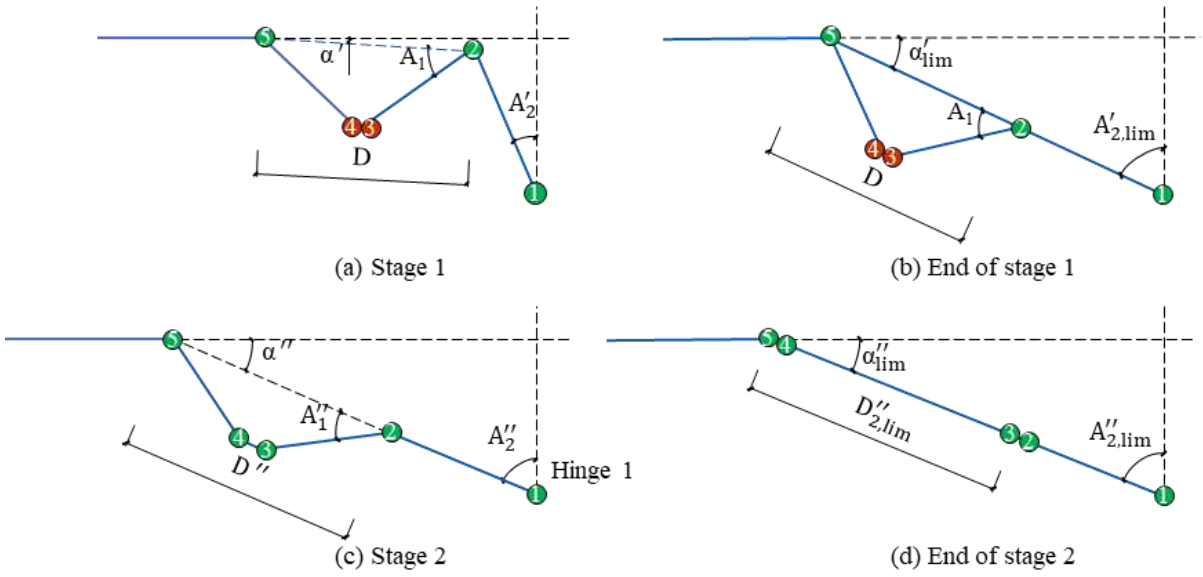

Figure 17. Pulling analytical model of Case 1.

The key to solving Equation (20) is to derive the relationship between the rotation of the control hinge and the total horizontal displacement. Since in the first stage only Hinges 1, 2 and 5 rotate, the distance D between Hinges 2 and 5 remains unchanged during this stage. If the rotation of Hinge 1, the control hinge in Stage 1, is θ, the angle α' can be calculated by Equation (21). According to the geometric relationship, the

rotations of Hinges 2 and 5 are $(\alpha'+\theta)$ and α', respectively. The total horizontal displacement and its increment can be obtained using Equations (22) and (23).

$$\alpha' = \arcsin\left[L_2 \left(\cos A_2 - \mathrm{Cos}(A_2+\theta)\right) / D \right] \tag{21}$$

$$\Delta = L_2 \left(\sin(A_2+\theta) - \sin A_2\right) + \sqrt{D^2 - L_2{}^2 \left(\cos A_2 - \mathrm{Cos}(A_2+\theta)\right)^2} - \mathrm{D} \tag{22}$$

$$\mathrm{d}\Delta = \left[L_2 \cos(A_2+\theta) + \frac{L_2{}^2 \sin(A_2+\theta)\left[\cos A_2 - \cos(A_2+\theta)\right]}{\sqrt{D^2 - L_2{}^2 \left[\mathrm{cosA}_2 - \mathrm{Cos}(A_2+\theta)\right]^2}} \right] d\theta \tag{23}$$

Stage 1 switches to Stage 2 when Hinges 1, 2 and 5 form a straight line, as shown in Figure 17 (b). Hinges 3 and 4 are then activated, and they will move towards the end hinges as the semi-cylindrical section is stretched. Hinge 2 is the control plastic hinge of Stage 2. Therefore, the rotation of Hinge 2 is firstly assumed, as β. Hinges 1, 2 and 5 always form a straight line. The distance D'' between Hinge 2 and Hinge 5 is calculated with Equation (24), using the tensile analytical model of the semi-cylindrical section developed in the previous paper [18].

$$D'' = D + 2r\left[n \sin\frac{\beta}{n} + \cos\beta - 1 \right] \tag{24}$$

where n is a parameter used to modify the calculation of the tensile deformation of semi-cylindrical section [18]. According to the geometric relationship, the rotations of Hinges 1, 3, 4 and 5 are $A_2'' - A_{2,\mathrm{lim}}'$, β, β and $\beta + A_2'' - A_{2,\mathrm{lim}}'$, respectively. The horizontal displacement and its increment in this stage can be calculated by Equations (25) and (26). The end of Stage 2 is when the component is stretched flat, shown in Figure 17 (d), and then the component is purely in tension. By substituting the relationship between the rotation of the control hinge and the total displacement into Equation (20), the force can be obtained. The first and second schemes of the component-based model are compared against the Abaqus in Figure 18.

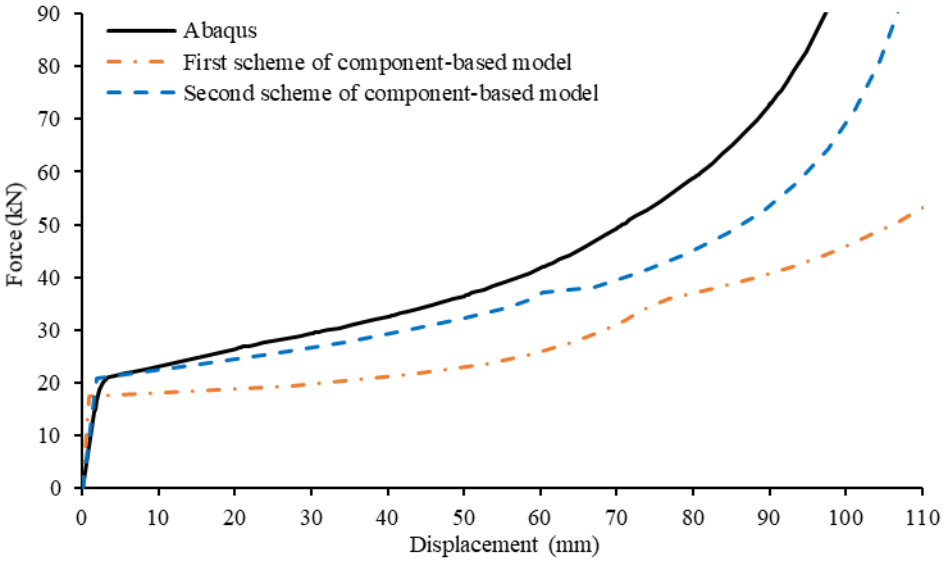

Figure 18. Pulling curves of Case 1 connection.

This figure shows that the second scheme of the component-based model matches the Abaqus results better than the first scheme, due to the application of the WCSC component. The kink in the blue dashed line representing the second scheme of the component-based model is caused by the transition from the first stage to the second stage.

$$\Delta = \sqrt{\left[D + 2r\left(n\sin\frac{\beta}{n} + \cos\beta - 1\right) + L_2\right]^2 - (L_2\cos A_2)^2} - L_2\sin A_2 - D \tag{25}$$

$$\mathrm{d}\Delta = \frac{\left[D + 2r\left(n\sin\frac{\beta}{n} + \cos\beta - 1\right) + L_2\right]\left[2r\left(\cos\frac{\beta}{n} - \sin\beta\right)\right]}{\sqrt{\left[D + 2r\left(n\sin\frac{\beta}{n} + \cos\beta - 1\right) + L_2\right]^2 - (L_2\cos A_2)^2}} \tag{26}$$

4.1.2 Push-back

Similarly to the first component-based model, the loading stage (loading, unloading, push-back or pull-back) of the WCSC component in the second scheme is still determined by the flowchart of Figure 13. For pushing back, there are two cases: 1) the component is pushed back from Stage 1 of pulling; and 2) the component is pushed back from Stage 2 of pulling.

If the component is pushed back from Stage 1 of pulling, the push-back deformation is the reverse process of the deformation of the first stage of pulling. The force-deformation relationship of the connection when it is pushed back from Stage 1 of pulling, from the Abaqus model and the two component-

based model schemes are shown in Figure 19. From the comparison shown in Figure 19, both the first and second component-based model schemes can produce results which are generally in agreement with the Abaqus simulation. The semi-cylindrical section of the Abaqus model deforms slightly (around 2mm) in the first stage of pulling. This is finally pushed back, causing the sudden kink towards the end of push-back. The second component-based model scheme assumes that the semi-cylindrical section does not deform during the Stage 1 of pulling, and so it cannot model this phenomenon.

The deformation process of the push-back of the connection from Stage 2 of pulling, simulated in Abaqus, is shown in Figure 20. This figure shows that the web cleat is pushed back to its original state at first, and then the semi-cylindrical section is pushed back. Therefore, the push-back of connection from Stage 2 of pulling includes two steps as shown in Figure 21.

The initial distance between Hinge 2 and Hinge 5 is related to the displacement D_{ref} at the reference point (when pushing back starts), and is calculated using Equation (27). In the first stage of push-back, the control plastic hinge is Hinge 1. Assuming that the rotation of Hinge 1 is θ_c, angle α_c' is calculated from Equation (28). Based on geometry, the rotations of Hinge 2 and Hinge 5 are $90° - \alpha_c' - A_{2,c}'$ and $90° - \alpha_c' - A_{2,c}' - \theta_c$, respectively. The total horizontal displacement and its increment are calculated using Equations (29) and (30). Stage 1 switches to Stage 2 when Hinge 2 has rotated back to the horizontal line passing through Hinge 5, as shown in Figure 21 (c). Stage 2 is the pushing back of the semi-cylindrical section. The analytical model of the semi-cylindrical section in compression developed in the previous paper [18] can be used here to calculate the force and displacement of the WCSC component.

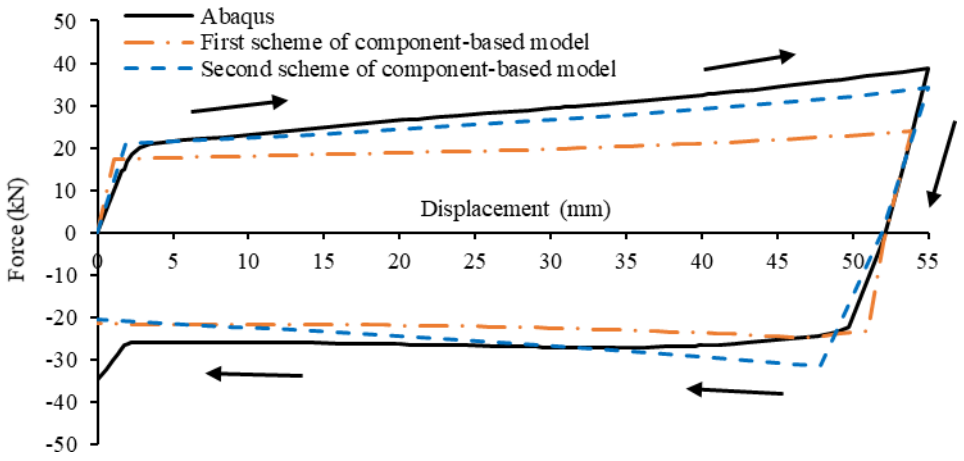

Figure 19. Push-back curves of Case 1 connection from Stage 1 of pulling.

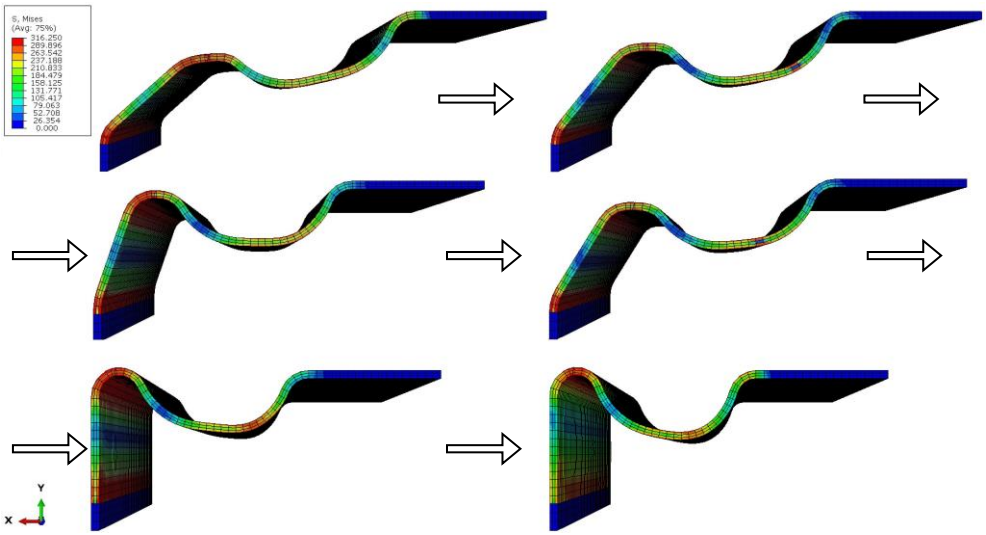

Figure 20. Deformation process of pushing back of connection from Stage 2.

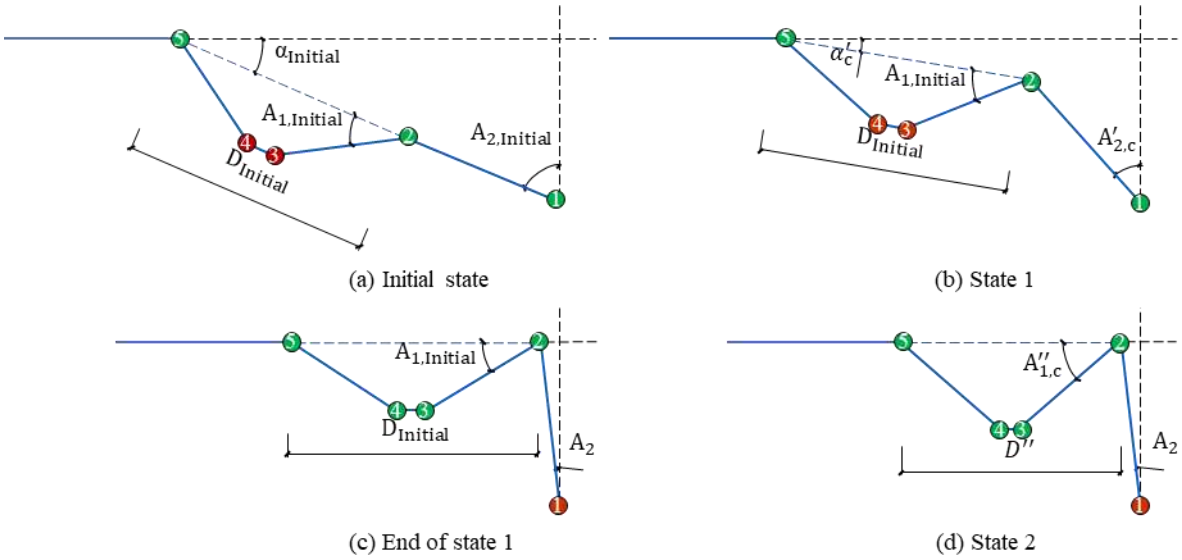

Figure 21. Push-back analytical model of Case 1 from Stage 2.

The force-displacement relationships of the connection when it is pushed back from Stage 2 of pulling, resulting from the first and second schemes of the component-based and Abaqus models are compared in Figure 22. The sudden increase of push-back forces shown in the figure indicates that the web cleat has been pushed-back to its original state, and the semi-cylindrical section has begun to be pushed back. The second component-based model scheme simulates the web cleat being pushed back to its original position earlier than for the other two models. This is because this model assumes that in the first stage of pushing back only the web cleat deforms, whereas the other two models also consider the tiny deformation of the semi-

cylindrical section at the same time, which is insignificant.

$$D_{Initial} = \sqrt{(D_{ref} + L_2 \sin A_2 + D)^2 + (L_2 \cos A_2)^2} - L_2 \tag{27}$$

$$\alpha_c' = \arcsin\left[L_2 \left(\cos A_2 - \mathrm{Cos}(A_{2,Initial} - \theta_c) \right) / D_{Initial} \right] \tag{28}$$

$$\Delta = D_{ref} - \left(D_{ref} + D + L_2 \sin A_2 - D_{Initial} \cos \alpha_c' - L_2 \sin A_{2,c}' \right) \tag{29}$$

$$d\Delta = L_2 \cos(A_{2,Initial} - \theta_c) - \frac{\left[L_2 \cos A_2 - L_2 \cos(A_{2,Initial} - \theta_c) \right] \cdot L_2 \sin(A_{2,Initial} - \theta_c)}{D_{Initial} \sqrt{D_{Initial}^2 - \left[L_2 \cos A_2 - L_2 \cos(A_{2,Initial} - \theta_c) \right]^2}} \tag{30}$$

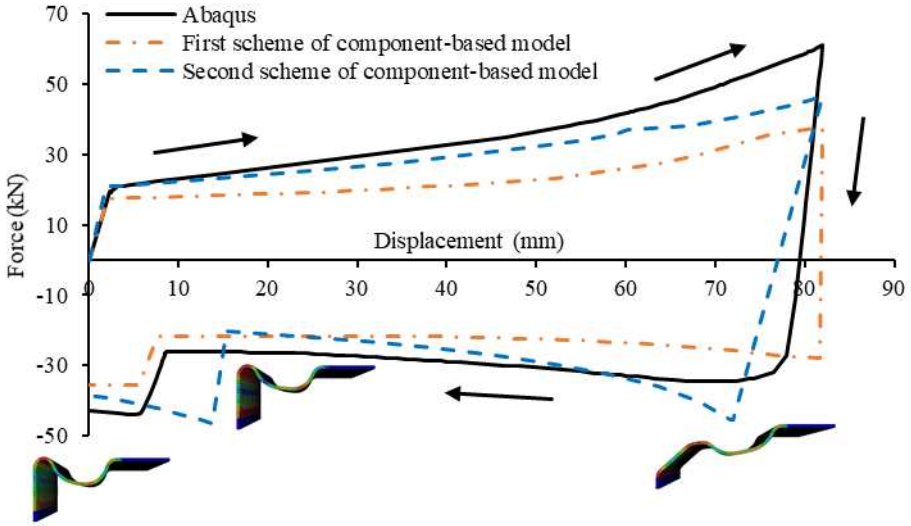

Figure 22. Push-back curves of Case 1 connection from Stage 2 of pulling.

4.2 Case 2 of the WCSC component

Similarly to Case 1, it is assumed that five plastic hinges can be formed during the deformation of the WCSC component, as shown in Figure 23. The key difference between Case 1 and Case 2 is that in Case 1 the length L_2 between Hinges 1 and 2 is larger than the radius of the semi-cylindrical section, whereas L_2 is smaller than the radius of the semi-cylindrical section in Case 2. The size of the example connection analysed in this section is shown in Figure 3 (b) and the dimension L_2 is equal to 46.6 mm.

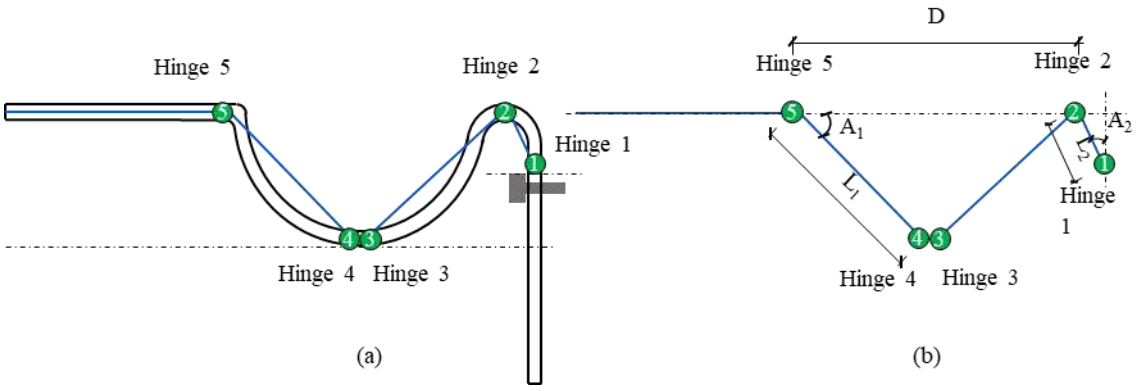

Figure 23. Schematic diagram of Case 2.

4.2.1 Pulling

The pulling of the WCSC component can be divided into two stages. In the first stage, only the semi-cylindrical component is stretched. In the second stage, all the plastic hinges rotate, as shown in Figure 24. The analytical model of the semi-cylindrical section in tension developed in the previous paper [18] is adopted here for the first stage of pulling. During the second stage, the behaviour of the hinges is more complex than that of Case 1. Therefore, the procedure shown in Figure 25 is followed to calculate the force and displacement of the component. At first, the rotation of Hinge 2 increases to β_i, and the length between Hinges 2 and 5 increases to D'', correspondingly. The force F_{axial} used to stretch the semi-cylindrical section is calculated. β_{max} represents the maximum rotation of Hinge 2 in the second stage, which is equal to A_2 minus the rotation of Hinge 2 in Stage 1. The rotation θ_j of Hinge 1 then increases while D'' remains unchanged. The maximum limit of θ_j, named as θ_{max}, is calculated from Equation (31); θ_{max} is reached when Hinges 1, 2 and 5 form a straight line. With the increase of θ_j, the force $F_{i,j}$ increases. However, θ_{max} may not be reached if $F_{i,j}$ is bigger than $F_{axial} \cdot \cos\alpha''$, which is the horizontal component of the force used to stretch the semi-cylindrical section. If $F_{i,j}$ is smaller than $F_{axial} \cdot \cos\alpha''$, the force $F_{i,j}$ and displacement $\Delta_{i,j}$ are output. Otherwise, the semi-cylindrical section will be further stretched, and the rotation of Hinge 2 will increase to β_{i+1}. As shown in Figure 26, the second component-based model scheme leads to a better comparison with the Abaqus result because of the WCSC component.

$$\theta_{\max,i} = \arcsin\left((L_2 \cos A_2) / (D" + L_2)\right) \tag{31}$$

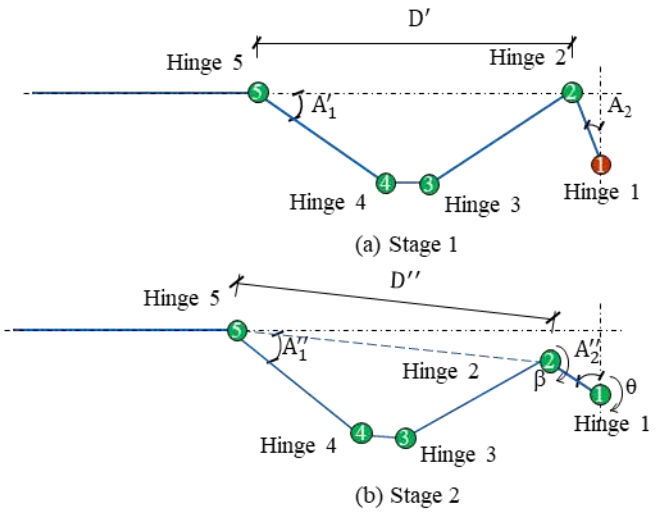

Figure 24. Analytical model of Case 2 in pulling.

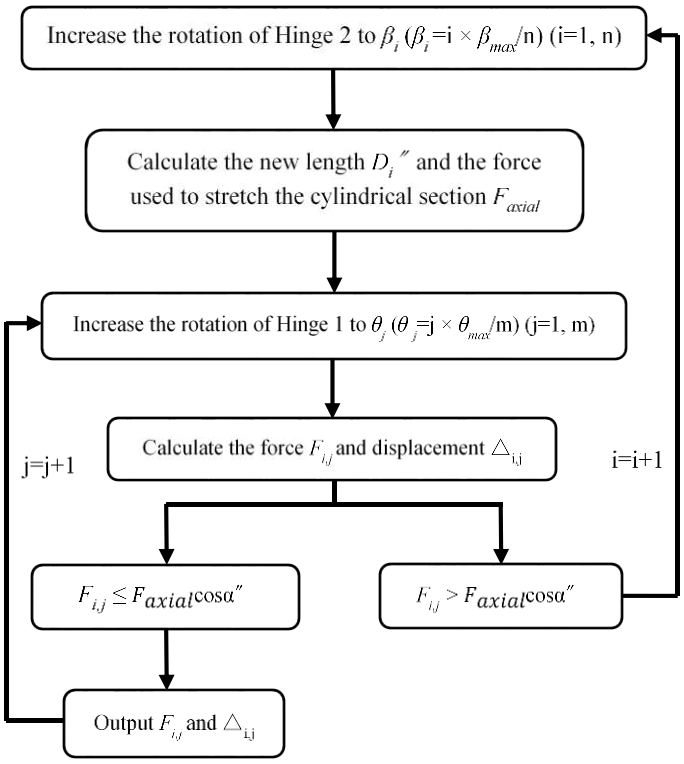

Figure 25. Calculation process of Stage 2.

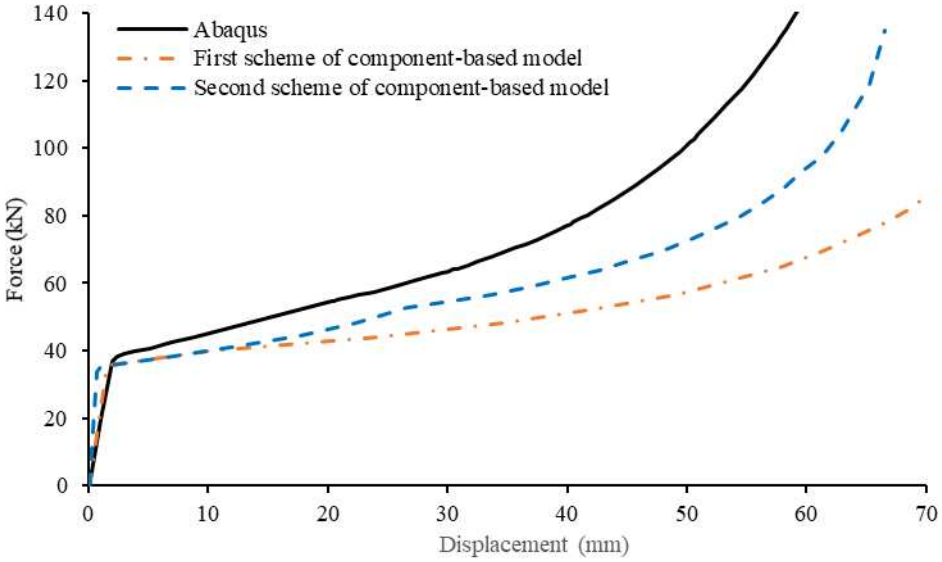

Figure 26. Pulling curves of Case 2 connection.

4.2.2 Push-back

There are two different situations of push-back in Case 2. When the connection is pushed back from the first stage of pulling, the analytical model of the semi-cylindrical section in compression developed in the previous paper is used to calculate the force and displacement of the WCSC component, as shown in Figure 27.

When the connection is pushed back from the second stage of pulling, the model developed for Case 1 is also applicable to Case 2. The push-back curve given by Case 2 of the second scheme of the component-based model is plotted in Figure 28, and compared with the first model and Abaqus. The resulting curves from the second scheme of component-based model is in better accordance with the Abaqus results.

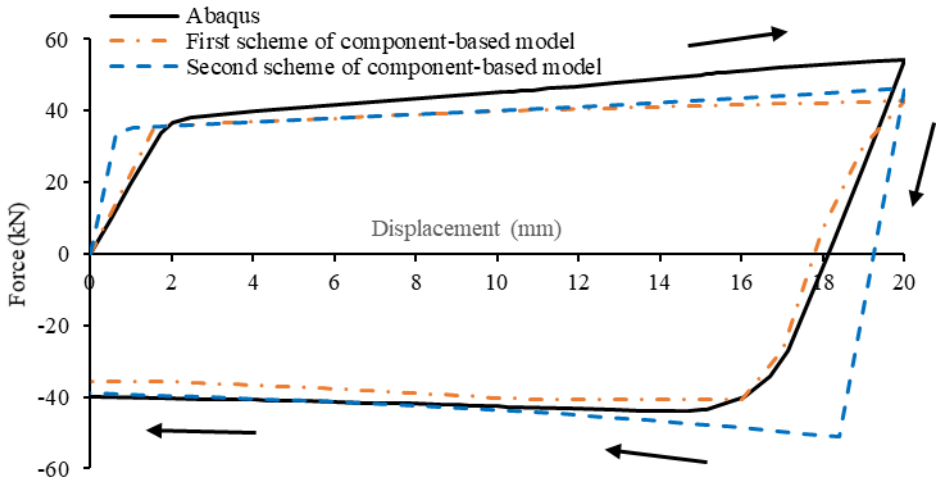

Figure 27. Push-back curves of Case 2 connection from Stage 1 of pulling.

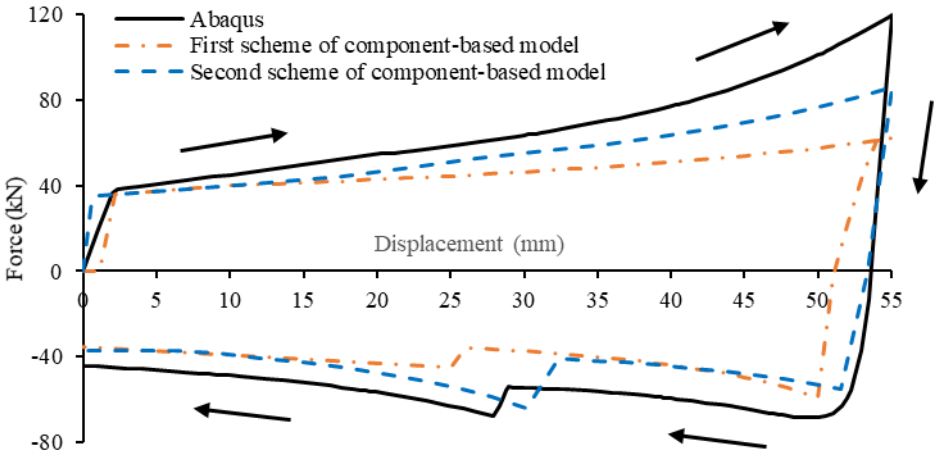

Figure 28. Push-back curves of Case 2 connection from Stage 2 of pulling.

4.3 Pushing and pull-back of the WCSC component

For pushing, when the component is pushed from its initial state, it is assumed that only the semi-cylindrical section deforms in both Cases 1 and 2. Therefore, the analytical model of the semi-cylindrical section in compression developed previously [18] is adopted for pushing of connection.

For pull-back after pushing, the pulling models developed for Cases 1 and 2 can still be used, except that the pre-deformed connection geometry needs to be considered. It should be noted that the choice of Case 1 or 2 for post-pushing pull-back needs to be re-assessed based on the deformed connection geometry. For instance, the appropriate case could be Case 1 for pulling but Case 2 for pulling back.

5. Comparison of the two component-based models against experiments

In this section, the experiments on model-scale connections conducted by Kalawadwala [23] are used for comparison with the two component-based model schemes proposed above. The dimensions of the tested specimens are documented in reference [18] and are not repeated here. Kalawadwala conducted three experiments, unloading from different levels of compression; -7.9mm (Experiment 1), -16.6mm (Experiment 2) and -24.0mm (Experiment 3). The deformed shapes of the specimens from all three experiments are similar; those of Experiment 3 are shown in Figure 29. Figure 29 (a) illustrates the initial state of the specimen and (b) shows the deformed shape and the beginning of unloading. Figure 29 (c) shows that the specimen is pulled back to its original state. Figure 29 (d) shows the specimen when it is eventually stretched flat. The experimental results, shown in Figure 30, Figure 31 and Figure 32, are compared with the Abaqus model and the two component-based model schemes. These figures show that the slope of the initial linear elastic

loading path and that of the unloading path given by the experiments are lower than those given by the Abaqus simulation and the component-based models. This may be because of slip between the clamps of the testing machine and the specimen. The pushing curves of the two component-based models are the same, since both assume that only the semi-cylindrical component deforms during pushing. The results of the second component-based model scheme are closer to the test and Abaqus than those of the first component-based model scheme.

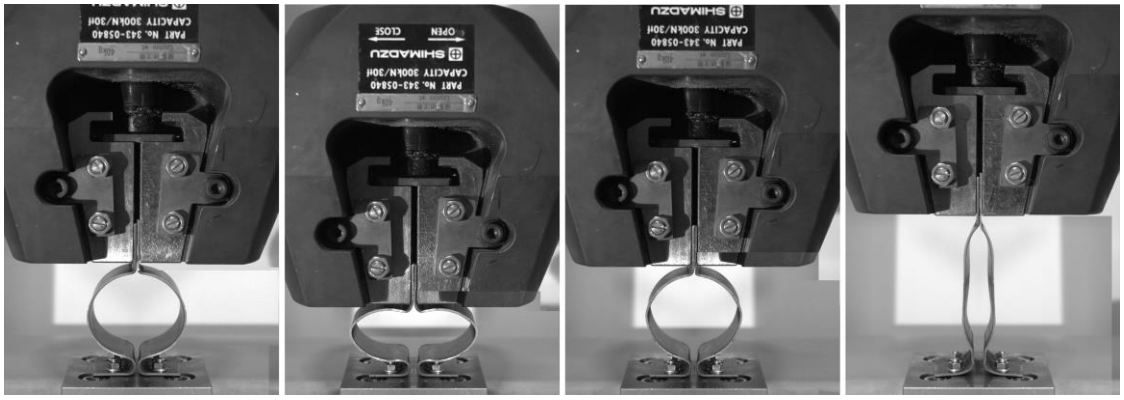

(a) Initial state (b) Pushing (c) Pull-back (d) Pulling

Figure 29. Experimental photos.

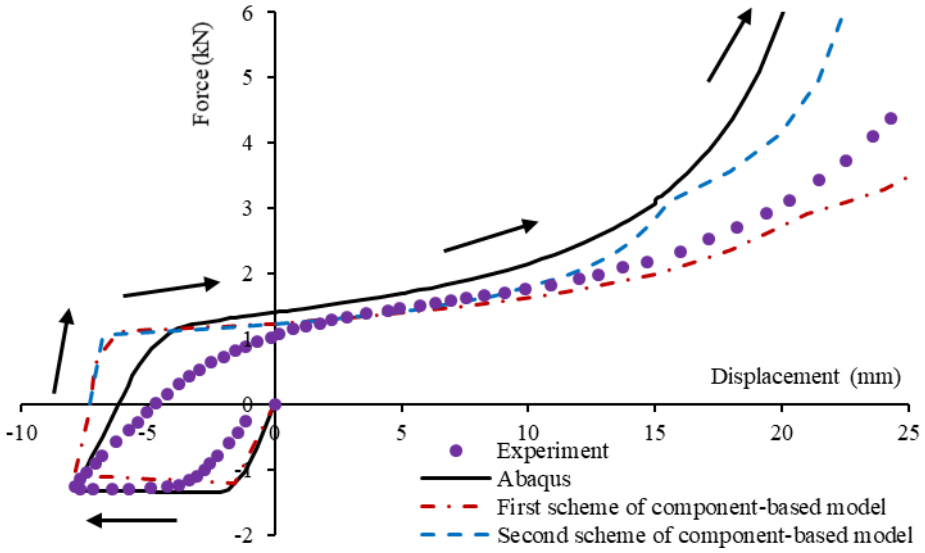

Figure 30. Experiment 1 results and modelling.

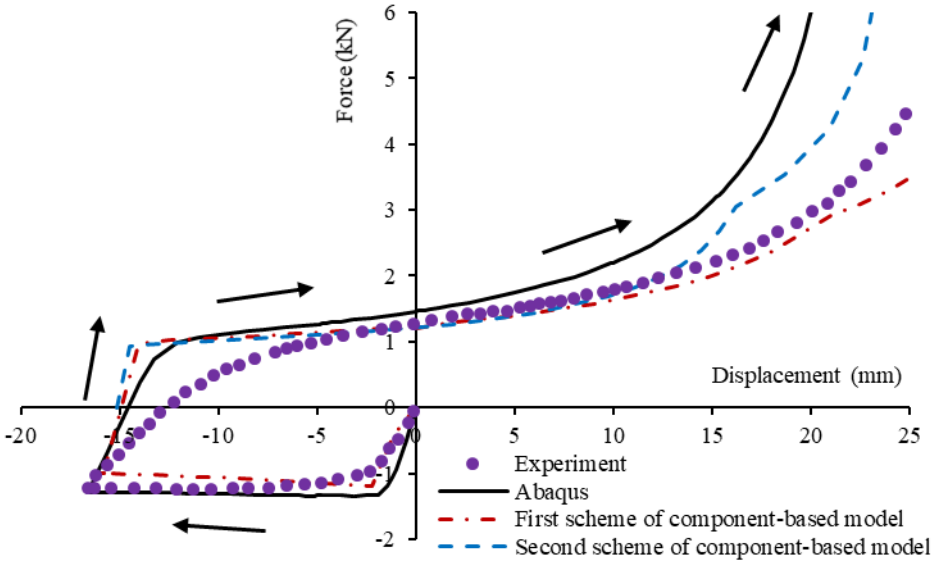

Figure 31. Experiment 2 results and modelling.

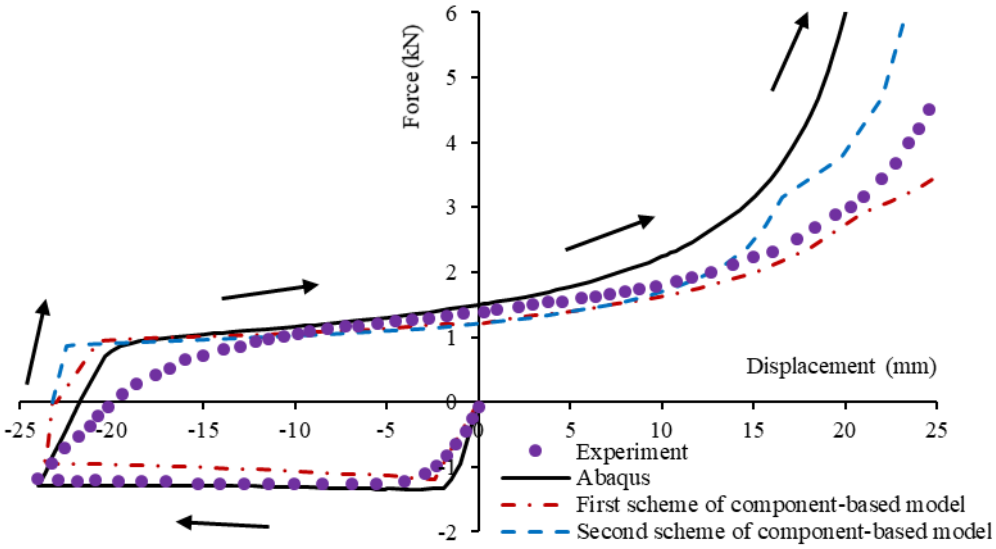

Figure 32. Experiment 3 results and modelling.

6. Example applications of the component-based model

The aim of the research is to implement the component-based model of the novel connection into global frame analysis in the near future. Before this is done, it is important to demonstrate how the model works in simulating isolated connections. Two load cases are discussed in this section. The above sections indicate that the second component-based model scheme delivers the better simulation results of the two, and so it is adopted in this section. As shown in Figure 33, a connection of the same dimensions as that shown in Figure

3 (b) is divided into five spring rows, each representing a bolt row. In Load Case 1, a horizontal tensile displacement is applied to the connection first, and then a rotation is applied to the centre line of the connection, with a centre of rotation as shown in the figure. In Load Case 2, a horizontal compressive displacement is applied first, followed by a similarly applied rotation. The results from Abaqus and the component-based model are compared in Figure 34. The force-displacement relationships of each spring row of these two cases are shown in Figure 35 and Figure 37. The force-rotation relationships of each spring row of these two cases are shown in Figure 36 and Figure 38.

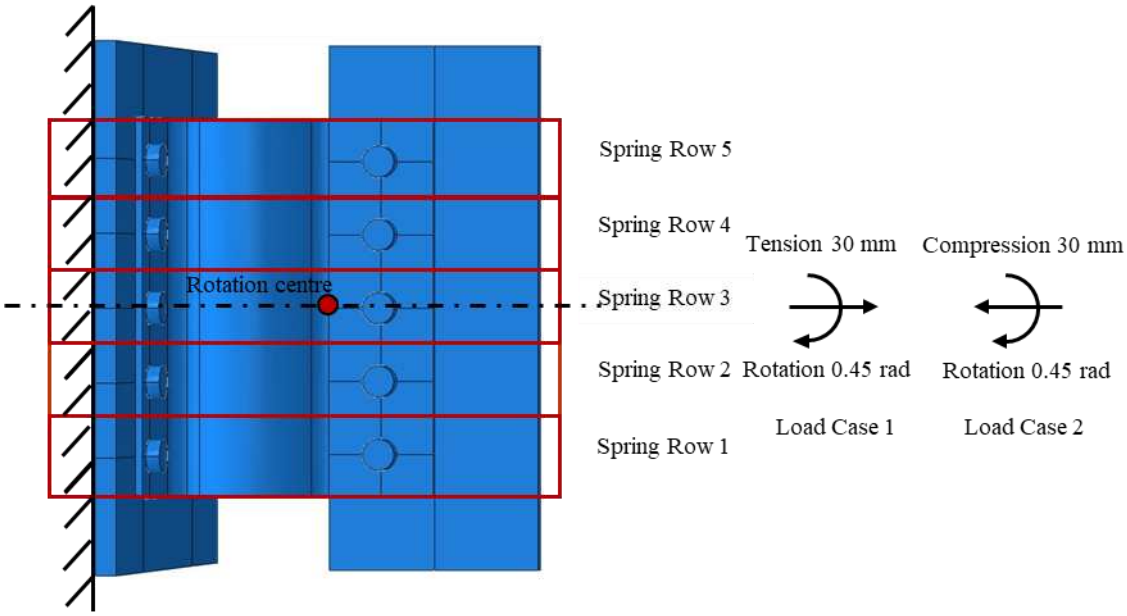

Figure 33. Division into 5 component rows for application examples.

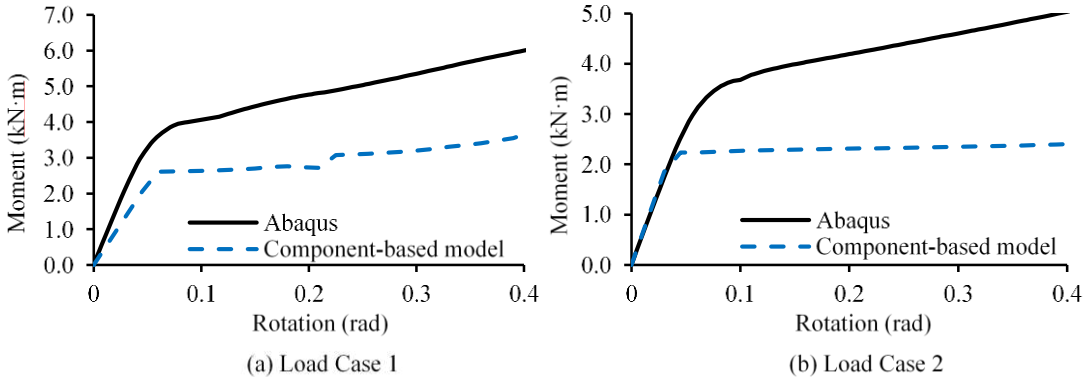

Figure 34. Comparison of moment generated with Abaqus simulations.

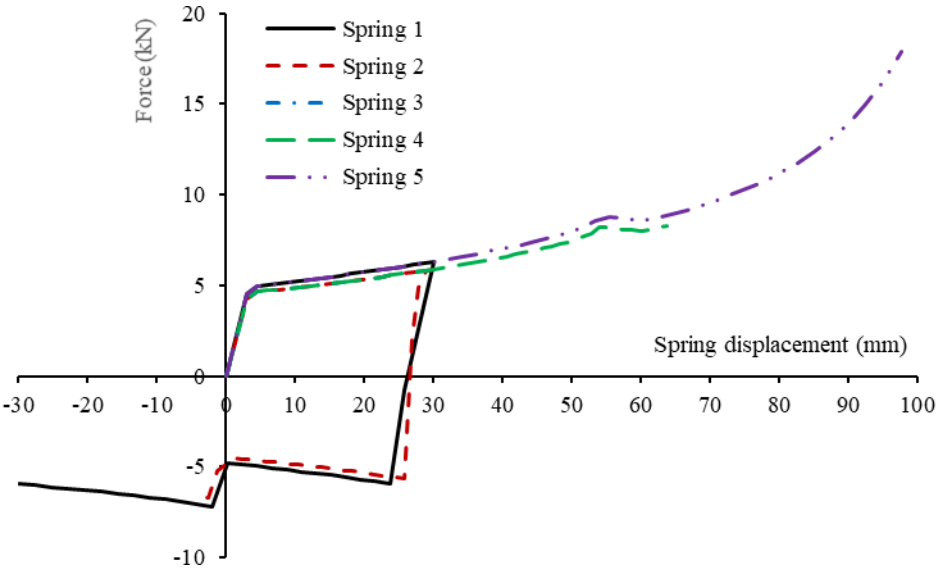

Figure 35. Force-displacement relationships of all spring rows in Load Case 1.

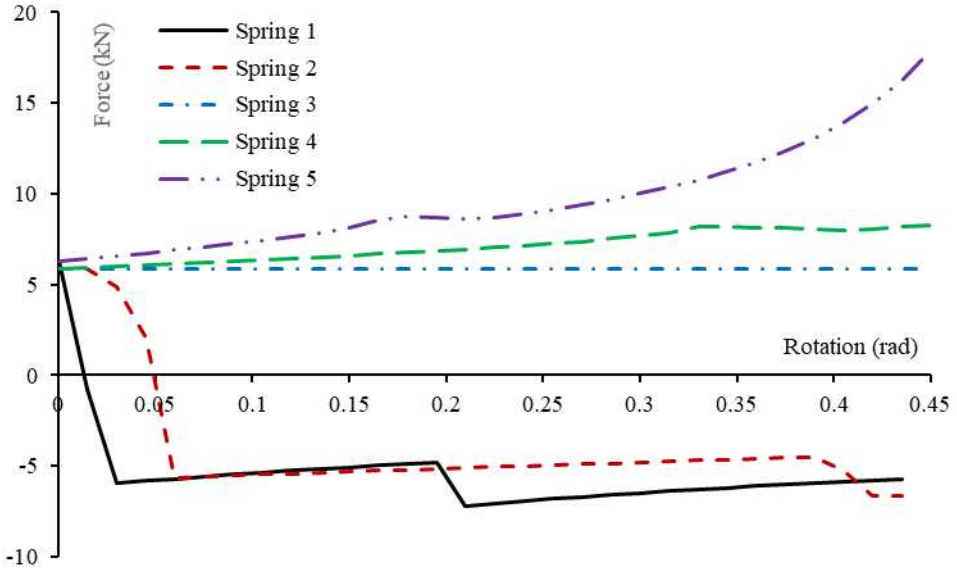

Figure 36. Force-rotation relationships of all spring rows in Load Case 1.

The discrepancy between the moment-rotation curves of the component-based model and Abaqus is quite large, as shown in Figure 34. This discrepancy may be due to the fact that torsion of the semi-cylindrical section and the semi-circular section of the web-cleat is ignored in the component-based model. The rotational behaviour of the entire connection consists of two actions, which are pulling/pushing of each spring row and torsion of the semi-cylindrical and semi-circular parts. However, it is very difficult to represent the torsional behaviour using an analytical model, since each bolt row is simultaneously subject to axial push/pull,

as well as torsion. In the context of the moment necessary to apply a significant rotation to the beam-end, the moment generated by applying the same rotation to the connection is small, and so an exact model of aspects such as torsion of the connection section is not very important to this study [18]. Deformation of two adjacent spring rows is only piecewise-compatible in the component-based model, which means that the horizontal shear force between adjacent spring rows is ignored. In Load Case 1, all spring rows experience pulling until 30 mm, at which stage the rotation is applied. With the increase of rotation, spring rows 1 and 2 undergo unloading, push-back and pushing, as shown in Figure 35 and Figure 36. The reason for the sudden increase of compressive force in both Spring Rows 1 and 2 at around 0 mm displacement is explained in Section 4.1.3, concerning pushing back from Stage 2 of pulling. Since Spring Row 3 is on the centre line of the connection, the applied rotation does not cause additional displacement to this row, and, therefore, the displacement of Spring Row 3 remains 30mm during rotation. Spring Rows 4 and 5 are always in tension (pulling) because they are above the centre line of the connection. In Load Case 2, all the spring rows are subject to 30 mm of compression (pushing) and then Spring Rows 4 and 5 switch to unloading, pull-back and finally pulling, as shown in Figure 37 and Figure 38. Spring Rows 1 and 2 are always under compression. Spring Row 3, on the connection centre line, maintains the compressive displacement of 30 mm during rotation.

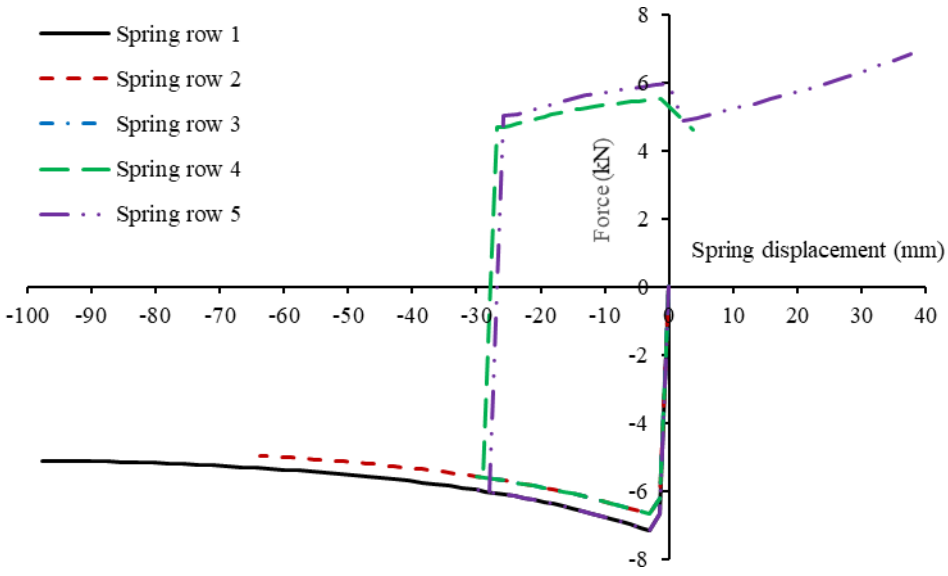

Figure 37. Force-displacement relationships of all spring rows in Load Case 2.

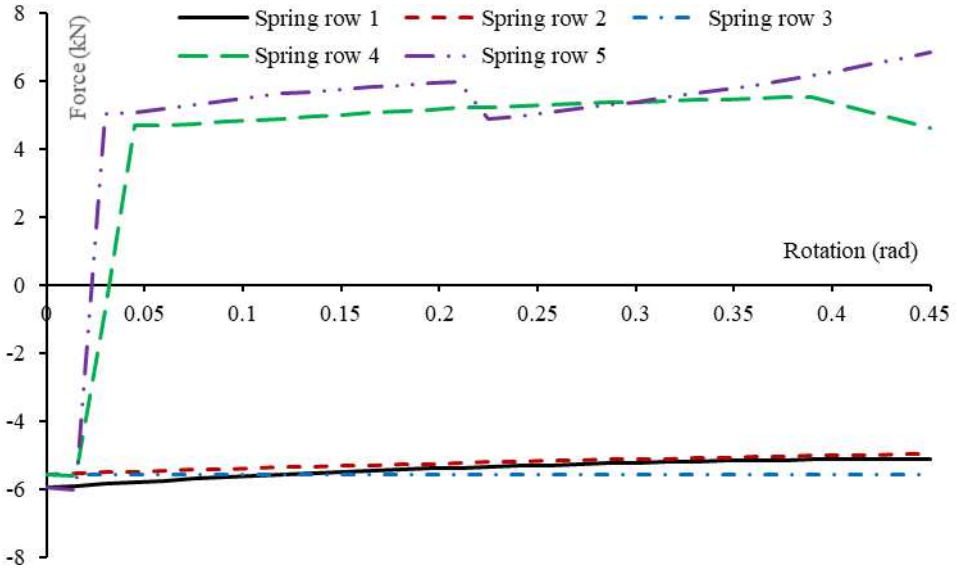

Figure 38. Force-rotation relationships of all spring rows in Load Case 2

7. Conclusion

This paper has introduced an improved design version of a novel ductile connection, which aims to enhance its practical feasibility of design and ease of fabrication. The performance of the improved connection was initially compared with that of the previous version using a sub-frame model. The comparison of the axial forces generated shows that the improved version produced smaller axial thrust than the previous version, which indicates an enhanced ductility. Five case studies were carried out, in which the novel connections were applied to sub-frames with different beam spans. These case studies illustrated the design requirements of the novel connection, and demonstrated the satisfactory deformation capacity of the novel connection by comparing the axial forces generated in the beams with novel connections with those of the beams with rigid connections.

The first analytical component-based model, including a web-cleat component model and a model of the semi-circular ductile part, based on simple plastic theory, was proposed. The 'Reference point' concept was adopted to describe the unloading behaviour of individual components, and this was developed to calculate the complete loading-unloading-reloading behaviour of the novel connection.

A second analytical model, the WCSC component, in which the semi-cylindrical component and the web-cleat component are considered to deform as a whole, was also developed. The resulting curves of the two schemes of component-based model have been compared against one another, as well as against Abaqus simulations and experiments. In general, the results from the second (WCSC) component-based model are

more in line with the behaviour given by Abaqus than those from the first model. Therefore, the second component-based model will be incorporated into the software Vulcan in the following work aimed at facilitating global frame analysis for structural fire engineering design.

Two preliminary application examples have investigated the performance of the proposed component-based model. There is some discrepancy between the results of the component-based model and Abaqus simulations, which is probably due to neglecting the torsion of the semi-cylindrical component parts of the component-based model. However, in a connection whose objective is to act essentially as non-moment-transmitting at ambient temperature and to permit a large amount of axial beam-end movement in fire, the moment resistance is more or less irrelevant, provided that it is low compared with the moment resistances of the connected members. However, the two simple examples illustrate how different spring rows work in the process of connection deformation.

References

[1] Liu T. Finite element modelling of behaviours of steel beams and connections in fire. Journal of Constructional Steel Research. 1996;36:181-99.
[2] Liu T. Moment-rotation-temperature characteristics of steel/composite connections. Journal of Structural Engineering. 1999;125:1188-97.
[3] Sarraj M, Burgess I, Davison J, Plank R. Finite element modelling of steel fin plate connections in fire. Fire Safety Journal. 2007;42:408-15.
[4] Sarraj M. The behaviour of steel fin plate connections in fire [PhD thesis]: University of Sheffield; 2007.
[5] Yu H, Burgess I, Davison J, Plank R. Numerical simulation of bolted steel connections in fire using explicit dynamic analysis. Journal of Constructional Steel Research. 2008;64:515-25.
[6] Al-Jabri KS. The behaviour of steel and composite beam-to-column connections in fire [PhD thesis]: University of Sheffield; 1999.
[7] Dai X, Wang Y, Bailey C. Numerical modelling of structural fire behaviour of restrained steel beam–column assemblies using typical joint types. Engineering Structures. 2010;32:2337-51.
[8] Garlock ME, Selamet S. Modeling and behavior of steel plate connections subject to various fire scenarios. Journal of Structural Engineering. 2010;136:897-906.
[9] Tschemmernegg F, Tautschnig A, Klein H, Braun C, Humer C. Zur nachgiebigkeit von rahmenknoten–Teil 1. Stahlbau. 1987;56:299-306.
[10] BSI E. 3: design of steel structures: part 1-8 design of joints, BS EN 1993-1-8. London: British Standard Institution. 2005;18.
[11] Jaspart J-P. General report: session on connections. Journal of Constructional Steel Research. 2000;55:69-89.
[12] Leston-Jones LC. The influence of semi-rigid connections on the performance of steel framed structures in fire [PhD thesis]: University of Sheffield; 1997.
[13] Block FM. Development of a component-based finite element for steel beam-to-column connections at elevated temperatures [PhD thesis]: University of Sheffield Sheffield, UK; 2006.
[14] Spyrou S. Development of a component based model of steel beam-to-column joints at elevated temperatures: University of Sheffield; 2002.

[15] Dong G, Burgess I, Davison B, Sun R. Development of a general component-based connection element for structural fire engineering analysis. Journal of Structural Fire Engineering. 2015;6:247-54.
[16] Hu Y, Davison B, Burgess I, Plank R. Component modelling of flexible end-plate connections in fire. International Journal of Steel Structures. 2009;9:1-15.
[17] Taib M, Burgess I. A component-based model for fin-plate connections in fire. Journal of Structural Fire Engineering. 2013;4:113-22.
[18] Liu Y, Huang S-S, Burgess I. Investigation of a steel connection to accommodate ductility demand of beams in fire. Journal of Constructional Steel Research. 2019;157:182-97.
[19] Gerstle KH. Effect of connections on frames. Journal of Constructional Steel Research. 1988;10:241-67.
[20] Franssen J-M. The unloading of building materials submitted to fire. Fire safety journal. 1990;3:213-27.
[21] El-Rimawi J, Burgess I, Plank R. The treatment of strain reversal in structural members during the cooling phase of a fire. Journal of constructional steel research. 1996;37:115-35.
[22] Bailey CG. Simulation of the structural behaviour of steel-framed buildings in fire [PhD thesis]: University of Sheffield; 1995.
[23] Kalawadwala S. Investigation of the performance of innovative connection under hazard loading. 2018.